Candida albicans' inorganic phosphate transport and evolutionary adaptation to phosphate scarcity

Maikel Acosta-Zaldívar*[1,2], Wanjun Qi*[1], Abhishek Mishra*[3], Udita Roy[1], William R. King[4], Jana Patton-Vogt[4], Matthew Z. Anderson[3,5], Julia R. Köhler[1,6]

1 Division of Infectious Diseases, Boston Children's Hospital/Harvard Medical School, Boston, MA 02115, USA
2 Current affiliation: Planasa, Valladolid, Spain
3 Center for Genomic Science Innovation, University of Wisconsin-Madison, Madison, WI
4 Department of Biological Sciences, Duquesne University, Pittsburgh, Pennsylvania, USA
5 Department of Medical Genetics, Laboratory of Genetics, University of Wisconsin-Madison, Madison, WI

6 Corresponding author

* These authors contributed equally.

macosta@planasa.com
Wanjun.Qi@childrens.harvard.edu
abhishek.mishra@wisc.edu
Udita.roy@childrens.harvard.edu
kingw@duq.edu
pattonvogt@duq.edu
mzanderson@wisc.edu
Julia.Koehler@childrens.harvard.edu

Abstract

Phosphorus is essential in all cells' structural, metabolic and regulatory functions. For fungal cells that import inorganic phosphate (Pi) up a steep concentration gradient, surface Pi transporters are critical capacitators of growth. Fungi must deploy Pi transporters that enable optimal Pi uptake in pH and Pi concentration ranges prevalent in their environments. Single, triple and quadruple mutants were used to characterize the four Pi transporters we identified for the human fungal pathogen *Candida albicans*, which must adapt to alkaline conditions during invasion of the host bloodstream and deep organs. A high-affinity Pi transporter, Pho84, was most efficient across the widest pH range while another, Pho89, showed high-affinity characteristics only within one pH unit of neutral. Two low-affinity Pi transporters, Pho87 and Fgr2, were active only in acidic conditions. Only Pho84 among the Pi transporters was clearly required in previously identified Pi-related functions including Target of Rapamycin Complex 1 signaling and hyphal growth. We used in vitro evolution and whole genome sequencing as an unbiased forward genetic approach to probe adaptation to prolonged Pi scarcity of two quadruple mutant lineages lacking all 4 Pi transporters. Lineage-specific genomic changes corresponded to divergent success of the two lineages in fitness recovery during Pi limitation. In this process, initial, large-scale genomic alterations like aneuploidies and loss of heterozygosity were eventually lost as populations presumably gained small-scale mutations. Severity of some phenotypes linked to Pi starvation, like cell wall stress hypersensitivity, decreased in parallel to evolving populations' fitness recovery in Pi scarcity, while that of others like membrane stress responses diverged from these fitness phenotypes. *C. albicans* therefore has diverse options to reconfigure Pi management during prolonged scarcity. Since Pi homeostasis differs substantially between fungi and humans, adaptive processes to Pi deprivation may harbor small-molecule targets that impact fungal growth and virulence.

Author Summary

Fungi must be able to access enough phosphate in order to invade the human body. Virulence of *Candida albicans*, the most common invasive human fungal pathogen, is known to decrease when one of the proteins that brings phosphate into the fungal cell, called Pho84, is disabled. We identified three more proteins in *C. albicans* that transport phosphate into the cell. We found that Pho84 plays the largest role among them across the broadest range of environmental conditions. After eliminating all 4 of these

transporters, we let two resulting mutants evolve for two months in limited phosphate and analyzed the growth and stress resistance of the resulting populations. We analyzed genomes of representative populations and found that early adaptations to phosphate scarcity occurred together with major changes to chromosome configurations. In later stages of the adaptation process, these large-scale changes disappeared as populations presumably gained small-scale mutations that increased cells' ability to grow in limited phosphate. Some but not all of these favorable mutations improved resistance of evolving populations to stressors like membrane- and cell wall stress. Pinpointing distinct mutation combinations that affect stress resistance differently in populations adapting to scarce phosphate, may identify useful antifungal drug targets.

Introduction

Phosphorus is an essential macronutrient for living cells and a major component of chromosomes, membranes and the transcription and translation machineries [1]. Inorganic phosphate (Pi) is required in the production of ATP, the energy currency of the cell, that governs central metabolic processes and intracellular signaling. Consequently, Pi is not only required for growth and proliferation but also for survival: e.g., fission yeast cells starved for Pi initially become quiescent and then lose viability [2].

Osmotrophic organisms that take up soluble small-molecule nutrients from their immediate environment must import Pi separately from molecular sources of nitrogen and carbon to acquire sufficient phosphorus. Most soils and aquatic environments contain <1%, or ≤10 mM soluble Pi, so that Pi is a scarce resource for plants and free-living microorganisms [3-5]; human serum Pi ranges from 0.8-1.3 mM [6], suggesting that microbial invasive pathogens of humans also experience Pi deprivation. For this reason, the Pi-homeostatic systems of small-molecule importing organisms like bacteria, plants and fungi have much in common. Orthology of phosphate proton symporters among plants and fungi was first determined by complementation of a *Saccharomyces cerevisiae* null mutant in *PHO84* with two *Arabidopsis thaliana* Pi transporters [7, 8]. In contrast, human phosphate homeostasis regulation differs fundamentally from that of osmotrophs [9, 10], and since abundant phosphorus-containing molecules are present in all human food sources of protein, the major high-affinity Pi transporter of fungi has no human homolog.

95 *Saccharomyces cerevisiae* Pi transporters were characterized over decades according to their Pi affinity
96 and their pH optima [11]. Kinetic studies in the 1980s identified two Pi transport systems, one with a low
97 K_m value of 8.4-21.4 µM, defined by the early investigators of these systems as high-affinity, and another
98 with a high K_m value of 0.77-1.7 mM, defined as low-affinity [12, 13]. Further analysis suggested two
99 separate transporters with distinct pH optima within the high-affinity uptake system [14]. Cloning and
100 functional characterization of the *PHO84* gene showed that its product is a component of the high-affinity
101 Pi transport system [15]. Heterologous expression of Pho84 and its incorporation into liposomes then
102 permitted kinetic studies that demonstrated a K_m for Pi of 24 µM [16]. *S. cerevisiae* Pho84 is a member of
103 the Phosphate: H^+ Symporter Family within the Major Facilitator Superfamily [17]; it uses the
104 chemiosmotic energy of proton symport to transport the Pi anion up a concentration gradient across the
105 plasma membrane.
106
107 Additional Pi import systems were subsequently identified and characterized. A separate high-affinity Pi
108 uptake system that was enhanced in the presence of sodium at pH 7.2 was described [18]; the gene
109 encoding this activity was later identified and its product, named Pho89, confirmed to have a Pi K_m of 0.5
110 µM [14]. Pho89 belongs to solute carrier family 20 as a sodium-dependent phosphate transporter [19, 20].
111 Low-affinity *S. cerevisiae* Pi transporters Pho87, Pho90 and Pho91 were subsequently characterized
112 genetically and functionally [21]. Pho91 was later shown to reside on the vacuolar membrane and
113 facilitate Pi export from the vacuole to the cytosol [22]. Further work showed distinct activities of the 2
114 low-affinity transporters: Pho87 versus Pho90 can sustain growth of *S. cerevisiae* down to Pi
115 concentrations of 5 mM versus 0.5 mM, respectively [23]. *S. cerevisiae* therefore has 2 high-affinity Pi
116 transporters, Pho84 and Pho89, whose energetic drivers are proton- and sodium symport, respectively,
117 and 2 paralogous low-affinity Pi transporters, Pho87 and Pho90 [21, 23].
118
119 The genome of the opportunistic fungal pathogen *Candida albicans* encodes 4 homologs of *S. cerevisiae*
120 Pi transporters. In a *mariner* transposon mutant screen we previously identified a mutant in the *C. albicans*
121 homolog of *S. cerevisiae PHO84* as hypersensitive to rapamycin [24]. We showed that *C. albicans PHO84*
122 is required in normal Target of Rapamycin Complex 1 (TORC1) signaling, oxidative- and cell wall stress
123 resistance, survival during exposure to amphotericin B and the echinocandin micafungin, and normal
124 virulence [24-26]. Given the presence of other Pi transporter homologs in the *C. albicans* genome, we

125 sought to understand how loss of just one, Pho84, could significantly impact important physiological
126 functions and even virulence in *C. albicans*.
127
128 Pi-acquisition and -homeostatic systems (PHO regulons) of bacterial and other fungal human pathogens
129 are required for virulence, implicating Pi scarcity as a prevalent condition in the host [27-30]: e.g., in a
130 pathogen that is completely adapted to its human host, *Mycobacterium tuberculosis*, transcription of a
131 secretion system for virulence factors is activated by Pi starvation [31, 32]. Expression of high-affinity Pi
132 transporters is typically regulated according to ambient Pi concentrations [33]. In *S. cerevisiae*, high-
133 affinity Pi transporter-encoding genes *PHO84* and *PHO89* are upregulated during Pi starvation [21, 34, 35].
134 In *C. albicans* ex vivo and in vivo infection models [36-40], the *PHO84* and *PHO89* homologs are similarly
135 upregulated [14]. These findings suggest that in the host, *C. albicans* like *M. tuberculosis* experiences Pi
136 starvation. We therefore set out to identify and characterize the other putative *C. albicans* Pi importers
137 that can contribute to cytosolic Pi availability for the fungus' growth and interaction with the host [24-26,
138 41].
139
140 We then asked whether *C. albicans* can adapt to persistent Pi scarcity. Forward genetic screens of
141 chemically or transposon-mutagenized cells subjected to specific selective conditions are powerful
142 discovery tools because they provide unbiased and often unexpected information [42]. In vitro evolution
143 and whole genome analysis has been used in other pathogens for the characterization of drug responses
144 [43-47] and in *Candida* species for analysis of drug resistance development [48-52]. We questioned
145 whether this approach might have benefits for analysis of adaptation to nutrient scarcity compared with
146 mutant screens. Its possible advantages might be a higher likelihood of revealing illuminating gain-of-
147 function mutations and the ability to uncover mutations involved in polygenic traits. We used in vitro
148 evolution and genome analysis to begin uncovering the cellular processes linked to *C. albicans'*
149 management of Pi scarcity.
150
151 **Results**
152
153 ***PHO84* plays a central role in growth and filamentation.**
154

155 Homology searches identified four Pi transporters in the *C. albicans* genome. A *C. albicans* ortholog of *S.*
156 *cerevisiae PHO89,* which encodes a high-affinity Pi transporter with an alkaline optimum [53], resides on
157 chromosome 4. Homology searches using the low affinity *S. cerevisiae PHO87* and *PHO90* paralogs found
158 a single homolog named *PHO87* in the Candida Genome Database (CGD) [53]. A *PHO84* homolog named
159 *FGR2* was also identified that shares 23% amino acid identity and 42% similarity with Pho84 (S1 Fig.). *FGR2*
160 was first isolated in a screen for *C. albicans* mutants impaired in filamentous growth [54] and more
161 recently found to contribute to filamentation differences between *C. albicans* strains [55]. To delineate
162 the contribution of these 4 predicted transporters to Pi acquisition, we constructed single gene deletion
163 mutants for *PHO89, PHO87* and *FGR2* using our FLP-*NAT1* system [56] to compare with our previously
164 constructed *pho84*-/- null mutants [24].
165
166 Pi restriction reduced growth only of *pho84*-/- mutants at acidic pH (Fig. 1). Null mutants in *PHO84* were
167 unable to grow on synthetic complete (SC) agar medium containing low (0.05 mM) or moderate (0.5 mM)
168 Pi at pH 3 or 5. In contrast, null mutants in the 3 other predicted Pi transporters grew similarly to the
169 wildtype control strain (WT) under these conditions, indicating that only *PHO84* is required in moderate
170 to low Pi at lower than neutral pH (Fig. 1; shown in Fig. 1 are also triple and quadruple mutants, which
171 retain only one or none of the 4 Pi transporters, respectively; these are described below in detail). At pH
172 7, *pho84* null mutants grew at all tested Pi concentrations, indicating that one or more other Pi
173 transporters were able to uptake sufficient Pi to sustain growth at neutral pH. At 7.3 mM Pi, all single
174 mutants in the 4 predicted Pi transporters grew robustly, indicating that no single transporter is
175 indispensable at high Pi concentrations (Fig. 1).
176
177 *C. albicans'* ability to readily switch between growth as single budding yeast versus as multicellular
178 filamentous hyphae contributes to its virulence [57, 58]. Cells lacking *PHO84* were previously shown to be
179 defective in hyphal formation [25, 59]. To examine the role of the different Pi transporters in
180 morphogenesis, cell suspensions from each of the 4 Pi transporter mutants were spotted on
181 filamentation-inducing agar media. Most clearly on Spider medium, cells lacking *PHO84* had minimal or
182 absent hyphal growth (Fig. 2A). Single mutants of the other 3 Pi transporters showed more subtle
183 filamentation defects than *pho84*-/- cells. Similar filamentation phenotypes were observed on RPMI agar
184 at pH 5 and pH 7: *pho84-/-* mutants produced occasional thin wisps of peripheral hyphae only on RPMI at
185 pH 5 but not pH 7, while *pho89-/-*, *pho87-/-* and *fgr2-/-* mutants showed robust hyphal growth on these

186 media (Fig. 2B). Together, these findings show that *PHO84* is the most important predicted Pi transporter
187 for filamentation under these conditions.
188
189 **Only *PHO84* impacted TORC1 signaling and oxidative stress endurance.**
190
191 We previously found that mutants in *PHO84* are hypersensitive to rapamycin and show decreased TORC1
192 signaling when growing in limited Pi [24], and that TORC1 co-regulates *PHO84* expression in addition to
193 its known regulation by Pho4 [60, 61]. TORC1 activation was reduced in *pho84-/-* cells as determined by
194 the phosphorylation state of ribosomal protein S6 (P-S6) [62] (Fig. 3) while null mutants of the other Pi
195 transporters did not show reduced P-S6. We concluded that Pho84 specifically contributes to TORC1
196 activation among the Pi transporters. TORC1 contributes to managing oxidative stress responses in *C.*
197 *albicans,* and mutants in *PHO84* are known to be hypersensitive to oxidative stress [25, 26, 59]. Among
198 single null mutants in each of the Pi transporters*,* only the *pho84-*/- mutant showed hypersensitivity to
199 the superoxide inducer plumbagin (S2 Fig.).
200
201 **Triple and quadruple mutants in predicted Pi transporters support a major role for Pho84.**
202
203 To examine the Pi uptake characteristics of each transporter, we constructed triple mutants that retained
204 one predicted Pi transporter, Pho84, Pho89, Pho87 or Fgr2. Triple mutants retaining a single Pi transporter
205 are abbreviated as the name of the sole remaining transporter followed by a capital A for "alone among
206 predicted Pi transporters" (e.g*.,* Pho84-A is *pho89-/- pho87-/- fgr2-/-*). Among these triple mutants, only
207 Pho84-A grew under all tested conditions (Fig. 1). Under Pi limiting conditions, Pho89-A cells showed
208 significant growth only at neutral pH. These results support a role for Pho89 as a high-affinity transporter
209 with a more alkaline optimum as in *S. cerevisiae* (Fig. 1). Pho87-A and Fgr2-A cells grew only in high Pi (7.3
210 mM) at acidic pH (pH 5 and pH 3) (Fig. 1), suggesting that Pho87 and Fgr2 are low-affinity transporters
211 with an acidic optimum.
212
213 We engineered two quadruple Pi transporter mutants (Q-, *pho84-/- pho89-/- pho87-/- fgr2-/-*). These
214 strains grew on rich complex medium, YPD, that contains organic phosphate compounds. They were then
215 tested for growth on Pi as the sole phosphorus source at a range of concentrations. Q- cells were able to
216 grow on high (7.3 mM) Pi at acidic pH, while on moderate (0.5 mM) Pi their growth was barely detectable

217 (Fig. 1). They did not grow at pH 7 or at a low Pi concentration (0.05 mM, Fig. 1). These findings show that
218 a residual Pi transport capacity exists in cells lacking the 4 identified Pi transporters that is active at high
219 Pi concentrations and at an acidic pH.
220
221 ***PHO84* supported growth under the broadest range of conditions.**
222
223 We defined the pH range at which each triple mutant retaining a single predicted Pi transporter was able
224 to grow in SC medium with low or high Pi. Growth was assayed by optical density and the area under each
225 growth curve (AUC) was depicted as a histogram (Fig. 4 and S3 Fig.). Substantial growth was defined as
226 growth ≥ AUC 5. Overall, we found that growth of Pho84-A (*pho89-/- pho87-/- fgr2-/-*) cells resembled
227 that of WT (Fig. 4), with growth optima between pH 2 and pH 7 in both high and low Pi conditions.
228
229 The role of Pho89 in growth was dependent on pH and Pi availability (Fig. 4). In low Pi, Pho89-A cells grew
230 equivalently to WT at pH 6 and above. In high Pi , Pho89 supported intermediate levels of growth at more
231 acidic pH and growth equivalent to WT at pH 6 and above. Pho89 could hence be described as a putative
232 high-affinity Pi transporter in neutral and alkaline conditions and a low-affinity transporter in acidic
233 conditions. *C. albicans*, like *S. cerevisiae*, therefore has two high-affinity Pi transporters, Pho84 and Pho89,
234 with the former having a broad pH activity range including in alkaline conditions, and the latter active at
235 pH ≥6.
236
237 Pho87 and Fgr2 were unable to support substantial growth in low ambient Pi and therefore are low-
238 affinity Pi transporters. Both supported growth only at acidic pH in high Pi. Pho87-A cells grew to an AUC
239 ≥5 only between pH 2 and 6, and even at their optimal conditions supported only ~70% of the WT growth
240 (Fig. 4). Fgr2-A cells showed the weakest growth with similar optima to Pho87-A cells, growing to an AUC
241 ≥5 only at pH 3 and 4 (Fig. 4). *C. albicans* therefore has two low-affinity Pi transporters, Pho87 and Fgr2,
242 with the latter, a Pho84 homolog, showing a narrow, acidic pH optimum.
243
244 Hyphal formation of triple Pi transporter mutants largely reflected the growth-sustaining properties of the
245 transporters. Q- mutants lacking all four Pi transporters failed to form hyphae under any conditions tested
246 (Fig 2). In contrast, Pho84-A cells encoding only Pho84 formed robust hyphae across all conditions (Fig. 2),
247 consistent with the strong hyphal defect of *pho84-/-* mutants. Pho89-A cells had severe hyphal growth

248 defects resembling those of *pho84-/-* mutants. Filamentation of the Pho87-A and Fgr2-A cells resembled
249 the Q- mutants (Fig. 2). These mutants did not grow sufficiently to form hyphae on RPMI buffered to pH
250 7 (Fig. 2C). Collectively, these findings are consistent with a concept that hyphal growth requires Pi uptake.
251
252 **Pho84 showed the most active Pi uptake under all tested pH conditions.**
253
254 In order to quantify the Pi transport capacity of each transporter, we performed Pi uptake experiments
255 with the triple mutants that each retained a single predicted transporter, by measuring Pi concentrations
256 remaining in culture medium over a time course. WT and Pho84-A cells removed Pi from the medium
257 rapidly and with almost identical kinetics (Fig. 5A,B). Pho89-A cells efficiently transported Pi at a narrow
258 range of pH 6-8, but their uptake dramatically slowed at pH 5 and below (Fig. 5C,D). These results support
259 a predominant role of Pho84 as the major Pi importer in *C. albicans,* while Pho89 makes a substantial
260 contribution around neutral pH.
261
262 Low-affinity Pi transporters Pho87 and Fgr2 showed slow Pi uptake under these conditions. Uptake of Pi
263 by Pho87-A cells was sluggish at pH 2-5 and almost undetectable at pH 6-9 (Fig. 5E). Despite known strong
264 induction of *FGR2* in low Pi conditions by Pho4, the transcriptional regulator of the PHO regulon [61], Pi
265 uptake by Fgr2-A cells was weak across the pH levels tested and these cells were unable to fully deplete
266 Pi from the medium at their pH 4 optimum (Fig. 5F). Both Pho87-A and Fgr2-A cells removed Pi from the
267 medium most rapidly at pH 4. Still, Pi uptake by Fgr2-A cells was significantly higher than that of Q- cells
268 at 30 hours (p=0.0001 by two-tailed t-test, Fig. 5G). These data support a role for Pho87 and Fgr2 as Pi
269 importers albeit with poor kinetics.
270
271 To identify any growth defects unrelated to Pi limitation in mutants containing a single Pi transporter, we
272 compared growth of triple mutants to WT in liquid YPD and Pi replete SC media. YPD contains organic as
273 well as inorganic phosphate sources, and SC contains high Pi concentrations (7.3 mM) and has an acidic
274 pH of 4-5 that favors activity of most Pi transporters. No triple mutants exhibited a growth defect in YPD
275 medium. In SC medium, Pho84-A grew as well as WT while Pho87-A, Pho89-A and Fgr2-A cells grew more
276 slowly (S4 Fig.), consistent with our previous results (Fig. 1 for SC medium with 7.3 mM Pi at pH 5). These
277 findings indicate that growth defects in these mutants correspond to a lack of Pi and not a nonspecific
278 fitness loss.

279

280 **Glycerophosphocholine transporters provided a minor Pi import function.**

281

282 To test whether *C. albicans* expresses additional Pi transporters that were not detected by our homology
283 searches, we next examined Q- cells for their ability to import Pi. At 30 hours, Q- mutants took up ~40%
284 of the Pi at pH 4 with efficiency being further reduced at pH 2, 5, 6 and 7 (Fig. 6A). These results
285 demonstrated that another low-capacity Pi transporting activity existed at low pH and high Pi
286 concentrations.

287

288 *C. albicans GIT3* and *GIT4* are distant *PHO84* homologs whose products import glycerophosphocholine
289 (GPC), a phospholipid degradation product that can serve as an organic source of phosphorus [63]. Once
290 in the cytosol, GPC is metabolized to glycerol, choline and phosphate under Pi limiting conditions [63]. The
291 GPC transporters Git3 and Git4 share 23% amino acid identity with Pho84 (41% and 39% similarity,
292 respectively, S1 Fig.). To test whether Git3 and Git4 might contribute to the residual Pi transport in Q-
293 cells, we competed Pi uptake by Git3 and Git4 with excess GPC in the medium. Addition of a 10-fold excess
294 of GPC completely eliminated Pi uptake by Q- cells (Fig. 6B). These findings support a role for Git3/4 in Pi
295 import at high ambient Pi and acidic pH.

296

297 We asked whether *C. albicans* has another modality to import Pi from its surroundings, in addition to the
298 2 high-affinity Pi transporters Pho84 and Pho89, the 2 low-affinity Pi transporters Pho87 and Fgr2, and the
299 GPC transporters Git3 and Git4. We engineered a septuple mutant strain "*tetO-PHO87"* that lacked three
300 Pi transporter homologs (*pho84-/- pho89-/- fgr2-/-*), GPC transporters that occupy adjacent loci on
301 chromosome 5 (*git2-/- git3-/- git4-/-*), and had a single tetracycline-repressible allele of *PHO87* (*pho87-*
302 */tetO-PHO87)*. Mutants were maintained without doxycycline to retain maximal expression of *PHO87*. A
303 role for Git2 in Pi import is currently not known; *GIT2* was deleted alongside the other two transporters
304 in their initial characterization and it was included in this construct to permit comparisons with mutants
305 described in Bishop et al. [63].

306

307 We reasoned that if a Pi-transporting activity remained in these cells, they would grow in Pi as their only
308 source of phosphorus, both in the absence and presence of doxycycline, i.e., during induction and
309 repression of *PHO87*. On the other hand, if we had mutated all transporters capable of importing sufficient

310 Pi to sustain growth, doxycycline exposure in SC media, devoid of organic phosphate sources, would
311 repress growth once internal Pi stores were depleted. We observed the latter result for the *tetO-PHO87*
312 septuple mutants (*pho87-/tetO-PHO87 pho84-/- pho89-/- fgr2-/- git2-/- git3-/- git4-/-*) (Fig. 6C). In
313 contrast at pH 3, an optimal pH for Pho87 activity, these mutants grew robustly in media without
314 doxycycline, YPD or normal SC (which contains high Pi, 7.3 mM) though they had a slight growth defect
315 compared to WT (Fig. 6C). Thus, the reduced growth of these mutants is largely attributable to Pi
316 starvation and not a consequence of a nonspecific fitness loss (S5A Fig.). We concluded that minimal Pi
317 import activity remains when *PHO84*, *PHO89*, *PHO87*, *FGR2* and *GIT2-4* have been genetically eliminated.
318

319 **In vitro evolution during Pi starvation restored growth in two distinct quadruple Pi transporter mutant**
320 **lineages**

321

322 We reasoned that in vitro evolution of *C. albicans* Q- mutants lacking all four Pi transporter homologs
323 (*pho84-/- pho89-/- pho87-/- fgr2-/-*) could reveal adaptive mechanisms that facilitate growth during Pi
324 scarcity. Our previous work showed that *pho84* null mutants' cell wall contained less phosphomannan and
325 had a thinner outer layer [26], suggesting that modifying cell wall structures while reserving scarce Pi for
326 essential processes like nucleic acid biosynthesis could sustain Pi-starved cells. We propagated two
327 lineages of the Q- mutants through 30 serial passages every other day in liquid SC medium with a
328 moderate concentration of 0.4 mM Pi. To reduce genetic bottlenecks, a large number of cells (~3.5×10^6
329 cells in 10 μl of saturated culture) were reinoculated into 10 ml of fresh medium. The population at each
330 passage was saved for DNA extraction and as a glycerol stock. During passaging, the growth rates of both
331 Q- lineages increased substantially and in distinct increments. Growth rates of the Q- lineages ultimately
332 plateaued before the end of the experiment. However, fitness recovery in the two lineages during
333 passaging differed significantly. Lineage 1 (Q- L1), evolving from JKC2830, recovered fitness more rapidly
334 and attained a growth rate similar to the WT by passage 24 (Fig. 7A). In contrast, growth rates of
335 populations derived from lineage 2 (Q- L2, evolving from JKC2860) remained lower than WT throughout
336 the experiment, plateauing at passage 20 (Fig. 7A). Fitness loss of Q- strains and fitness recovery of their
337 descendant passaged populations was specific to Pi scarcity. In YPD, both Q- strains and their 30th passage
338 descendant populations grew robustly (S5B Fig.). These findings indicated that *C. albicans* cells lacking Pi
339 transporters could recover fitness during prolonged Pi deprivation, and that this adaption did not lead to
340 fitness loss when the selective pressure was relieved.

341

342 **Acquisition and loss of aneuploidies accompanied adaptation of evolving Q- lineages to Pi scarcity.**

343

344 To uncover the underlying genomic changes associated with improved growth of evolving Q- strains, we
345 performed whole genome sequencing of the WT ancestral to the Pi transporter mutants (JKC915), as well
346 as cell populations of selected passages from both lineages, Q- L1 and Q- L2. Populations that bounded
347 significant fitness gains were chosen for sequencing, generating genomic snapshots of the evolved
348 population for passages 4, 13, 18, 19, and 30 of Q- L1, and passages 5, 7, 19, 24, and 30 for Q- L2.

349

350 Major chromosomal rearrangements occurred during construction of the Q- mutants and during their
351 passaging. The WT strain used to construct the Q- mutant lineages was diploid with no evidence of
352 segmental copy number variations or large loss of heterozygosity (LOH) tracts. The genomes of both Q-
353 strains were trisomic for chromosome 5 (Chr5, Fig. 7B), which includes *GIT2-4*. This aneuploidy was
354 accompanied by LOH tracts on the left arm of Chr2 (Chr2L) and Chr3R, neither of which include loci
355 disrupted in the Q- mutant. LOH of Chr2 resulted in homozygosis of the A allele for >50% of the
356 chromosome, and LOH of Chr3 produced a short tract of homozygosity for B alleles (Fig. 7B).

357

358 Both evolving lineages acquired similar large-scale genomic changes during adaptation to Pi scarcity. Each
359 lineage independently acquired a Chr2 trisomy, first seen in passage 13 and passage 19 for Q- L1 and Q-
360 L2, respectively (Fig. 8). The Chr2 trisomy was subsequently largely or partially lost in Q- L1 and Q- L2,
361 respectively, possibly as populations accumulated fitness-enhancing small-scale mutations. The Chr5
362 trisomy was also lost during passaging of Q- L1, likely due to fitness defects associated with aneuploidy
363 (Fig. 8).

364

365 Persistence of Q- L2's segmental aneuploidy on the left arm of Chr2 (Fig. 8) by the 30th passage suggests
366 potential adaptive contributions of the encoded loci. This amplified region of Chr2 ranged from nt
367 1,316,396 to 1,617,025 and encompassed 147 open reading frames. Manual annotation of these genes
368 (SI Table 1) identified *GIT1,* which encodes a glycerophosphoinositol permease [64] with 22% amino acid
369 sequence identity to Pho84. There is experimental evidence against a role of Git1 in Pi transport in *C.*
370 *albicans* [64] but its role in phosphorus homeostasis might be indirect, i.e. by facilitating
371 glycerophosphoinositol uptake as Pi starvation induces plasma membrane remodeling [65].

372

373 **Specific stress phenotypes of Q- population passages did not consistently correspond to their fitness in**
374 **Pi scarcity.**

375

376 As we previously found hypersensitivity of *pho84* null mutants to rapamycin as well as oxidative-, cell wall-
377 and membrane stress, induced through plumbagin, micafungin and amphotericin exposure respectively
378 [24, 26], we investigated these responses in the Q- mutants and their evolved lineages. WT, both Q- strains
379 and their passage 30 descendant populations were grown in liquid medium; these strains and in addition,
380 populations from intermediate passages from the evolution experiment were spotted as serial dilutions
381 onto solid medium in the absence or presence of these stressors. Q- mutants were hypersensitive to
382 membrane stress induced by amphotericin and SDS and to cell wall stress induced by micafungin; they
383 showed rapamycin sensitivity corresponding to their growth defects in vehicle (Fig. 9).

384

385 In contrast, the responses of evolved, late-passage Q- L1 and Q- L2 populations were distinct for each
386 stressor. Q- L1 but not Q- L2 populations regained growth rates in amphotericin almost to WT levels by
387 passage 30 (Fig. 9A,B). The Q- L2 passage 30 population had increased sensitivity to SDS, compared with
388 its ancestral Q- L2 strain (Fig. 9A,B) while its Q- L1 counterpart regained the ability to grow in the presence
389 of SDS almost to the level of the WT (Fig. 9A,B). In the presence of micafungin, growth of selected passages
390 reflected their fitness in Pi-limited medium (Fig. 9C). However, Q- L1 but not Q- L2 passaged populations
391 regained growth in plumbagin while conversely, Q- L2 populations evolved frank resistance to rapamycin
392 by passage 30 (Fig. 9C). Like the different fitness levels in Pi scarcity reached by the end of the experiment,
393 the distinct stress phenotypes of Pi scarcity-adapted populations suggest their evolutionary trajectories
394 had diverged.

395

396 **Discussion**

397

398 In this work, we characterized 4 predicted *C. albicans* Pi transporters, Pho84, Pho89, Pho87 and Fgr2,
399 identified by sequence homology, and determined their contributions to Pi acquisition. In brief, among
400 the high-affinity Pi transporters, Pho84 was the most important for growth, filamentation, stress
401 responses, and induction of TORC1 signaling and had the broadest pH range of Pi uptake capacity, while
402 Pho89 was specialized for uptake in neutral and alkaline pH (Table 1). Among the low-affinity Pi

403 transporters, both of which were only active at acidic pH, Pho87 was more efficient and had a broader pH
404 range while Fgr2 functioned only between pH 3 and 5 (Figs. 4, 5). In contrast to *S. cerevisiae*, *C. albicans*
405 low-affinity Pi transporters are not paralogs; rather, the less efficient one, Fgr2, is a distant Pho84
406 homolog. The minor role for Fgr2 in *C. albicans* Pi import stands in contrast to *Cryptococcus neoformans*
407 where both *PHO84* homologs (*PHO84* and *PHO840*) make significant contributions to Pi transport [66]. In
408 the absence of all specific Pi transporters, glycerophosphocholine transporters were able to provide
409 residual Pi import to sustain growth. Cells lacking all Pi transporters were able to regain fitness during
410 sequential passaging in limited Pi, that plateaued at distinct levels for 2 populations in accordance with
411 previously described declining adaptability [67, 68], while engendering distinct responses to some Pi-
412 relevant stressors. During the evolution experiment, similar large-scale genomic changes were
413 sequentially acquired and partially or completely lost in the 2 independently evolving populations.
414 Retention of a segmental amplification within Chr2 in the less fit lineage suggests that genes in this
415 trisomic region may contribute to fitness in limited Pi but the precise loci responsible remain undefined.
416
417 The severe growth defect of Q- cells that lack all 4 identified Pi transporters argues against the presence
418 of other specific Pi transporters. Q- cells removed a small fraction of the Pi present in their medium. The
419 glycerophosphocholine transporters Git3 and 4 provided minor transport activity that was most evident
420 in the growth difference between a Q- mutant and the septuple mutant when grown in the presence of
421 doxycycline to repress *PHO87* (Fig. 6C). The ability of GPC provision to completely outcompete measurable
422 Pi uptake in Q- cells (Fig. 6B) also argues against other cell surface transporters beside Git3 and Git4 playing
423 a measurable role in Pi uptake under our experimental conditions.
424
425 pH sensitivity is a key feature of each transporter. Like WT, Pho84-A, Pho87-A, and Fgr2-A cells grew
426 optimally between pH 3 and 6. Only cells expressing *PHO89* alone showed a growth optimum between pH
427 6 and 8. The pH of the oral and pharyngeal mucosa as well as most of the gastrointestinal tract colonized
428 by *C. albicans* is broadly neutral or alkaline, though mucosal microenvironments may be acidic due to
429 bacterial metabolites. During acute invasive disease, *C. albicans* finds itself in mildly alkaline blood and
430 tissue environments between pH 7.35 and 7.45. Pi acquisition systems of *C. albicans* are therefore not
431 well adapted to host environments encountered during invasive disease. The reduced Pi transport activity
432 at alkaline pH of the bloodstream might explain why the PHO regulon is induced during systemic disease,
433 reflecting “alkaline pH-simulated nutrient deprivation” [69], despite the presence of abundant Pi and

434 organic phosphate compounds like GPC. Pi import is also critical for proliferation of other human fungal
435 pathogens [30, 70, 71] and unicellular parasites [72] each of which must contend with neutral to alkaline
436 conditions in host deep organs.
437
438 Loss of *PHO84* but not of the other Pi transporters had a substantial effect on TORC1 activity (Fig. 3) and
439 oxidative stress endurance (S2 Fig.). These experiments cannot distinguish between specific activities of
440 Pho84 in these cellular functions, versus the predominant role of Pho84 in providing Pi to the cell. We
441 found in another context that TORC1 activity depends on availability of Pi but not on the presence of
442 Pho84, while endurance of peroxide stress may require an activity specifically of Pho84 [73]. *C. albicans*
443 *PHO84* transcription is co-regulated by TORC1 in addition to Pho4 [24], but how these systems interact
444 and modulate each others' outputs remains unknown.
445
446 Hyphal growth defects mirrored the severity of Pi transport deficiency among the constructed mutants.
447 Among the Pi transporters assayed in defined mutants, only Pho84-A cells produced robust hyphae on all
448 3 media examined (Fig. 2), while Pho87-A cells produced some hyphae on RPMI pH 5, and Pho89-A cells
449 had sparse, short hyphae on RPMI pH 7 (Fig. 2). The role of Pi uptake in filamentation might be indirect,
450 through activation of signaling systems like TORC1 required for hyphal morphogenesis [74]. Alternatively,
451 given the larger surface area of hyphal cells compared to yeast cells, hyphal cells must consume larger
452 amounts of phosphoric metabolites like nucleotide sugars required as building blocks for the cell wall. The
453 inability to produce sufficient phosphorus-containing intermediates might inhibit hyphal morphogenesis
454 to minimize cell wall surface area and preserve phosphorus for other vital functions.
455
456 To probe *C. albicans'* options for adaptation to Pi scarcity, we performed an in vitro evolution experiment
457 with Q- strains in which we had deleted the known Pi transporters. These strains had acquired, at an
458 unknown point during their construction, a trisomy of Chr5 where the genes encoding organic phosphate
459 transporters Git3 and Git4 reside. *C. albicans* GPC transporters are upregulated by the transcription factor
460 Pho4 during Pi starvation [61]. As Q- cells grew very poorly in medium with a moderate Pi content of 0.4
461 mM, increasing the gene dosage of *GIT3* and *GIT4* by retaining a third copy of Chr5 still did not restore
462 significant Pi uptake, as shown in Fig. 5G. During the evolution experiment, a further large-scale genomic
463 alteration appeared in both lineages: triploidy of Chr2 with simultaneous LOH reducing all 3 alleles to AAA

464 in a long segment on the left arm of the chromosome (cyan-colored segment of Chr2 in both lineages, Fig.
465 8).
466
467 When abruptly exposed to significant stress, *C. albicans* is known to frequently resort to aneuploidy and
468 LOH to provide a crude but rapid option to improve fitness specific to the particular stress [48-50, 75, 76],
469 reviewed in [77]. Ploidy increases that enhance fitness under specific stress conditions can be achieved
470 more rapidly than accumulation of advantageous (in the setting of the specific stress) point mutations
471 because chromosome missegregation occurs once every 5×10^5 cell divisions (in *S. cerevisia*e) [78] while
472 substitution of any particular base pair is estimated to occur once every 1.2×10^{10} cell divisions in *C.*
473 *albicans* [79] and every 1.67×10^{10} cell divisions in *S. cerevisiae* [80]. Populations under strong selection
474 are therefore more likely to initially become enriched for aneuploid mutants than for cells containing
475 constellations of advantageous point mutations [81]. Large-scale copy number variants like trisomies
476 however incur fitness costs due to increased transcription and translation of a multitude of genes that
477 result in excess protein production and protein complex stoichiometry imbalances [78, 82, 83]. These
478 fitness costs predominate when the selective pressure of the stress relents [48, 83]. In addition to
479 environmental changes that diminish stress intensity, small-scale genomic changes (like single nucleotide
480 mutations and small insertions or deletions) that promote adaptation to the specific stressor can relieve
481 selective pressure and favor loss of a trisomic chromosome. For example, a gain-of-function point
482 mutation of a transcriptional regulator [48, 84], may alleviate a specific stressors' selective pressure to the
483 point that trisomies resolve back to diploid, as we observed in the Q- L1 but not the Q- L2 lineage.
484
485 Evolving quadruple Pi transporter mutants similarly gained trisomies in both independent populations,
486 highlighting the strong selection experienced by these cells. Loss of trisomies during passaging may have
487 been enabled by accumulating fitness-enhancing small-scale variants. The distinct mutations that
488 permitted these adaptive solutions remain to be identified. Given their cell wall- and membrane stress
489 response phenotypes, it is tempting to speculate that Pi-sparing modifications of membranes and the cell
490 wall might increase fitness during Pi scarcity. The cyanobacterium *Prochlorococcus,* a dominant species in
491 waters of the North Pacific Subtropical Gyre, has a competitive advantage in this Pi-scarce ecosystem due
492 to its membrane composition largely of sulfo- and glycolipids, in which fatty acids are linked to
493 sulfate/sugar- or sugar-based, instead of phosphate-based, polar head groups [85]; other phytoplankton
494 use similar adaptations [4]. *C. albicans* also economizes on non-essential uses of Pi by remodeling its

495 membrane systems: the gene encoding a homolog of diacylglyceryl-*N*,*N*,*N*-trimethylhomoserine synthase
496 is strongly upregulated during Pi starvation in dependence on the PHO regulon [61] and like *Neurospora*
497 *crassa* and *C. neoformans, C. albicans* can replace membrane phospholipids with betaine-headgroup lipids
498 during Pi starvation [65, 86].
499
500 A caveat is that the distinct stress phenotypes of the two passage 30 populations could be incidental or
501 integral to their Pi management strategies. Detailed genotype comparisons and further genetic and cell
502 biologic analysis of distinct mutations in the two lineages will be required to test causal relationships
503 between the phenotypes. For example, while distinct SDS stress phenotypes and distinct strategies to Pi
504 scarcity adaptation could be unrelated, another possibility is that the overall genomic changes that
505 occurred in the Q- L2 during Pi scarcity adaptation led to membrane changes that rendered it susceptible
506 to detergent stress from SDS. In contrast, the adaptation trajectory of lineage Q- L1 may have required
507 less changes to membrane composition so that its SDS endurance was restored as it adapted to growth in
508 scarce Pi. Genetic, genomic and lipidomic analyses will be required to distinguish these possibilities.
509
510 These experiments have several limitations. As noted, there was a residual Pi transport activity in addition
511 to the predicted Pi transporters present in triple mutant cells due to presence of GPC transporters Git3
512 and Git4; this residual activity was minor, though, and only detectable at high ambient Pi and acidic pH.
513 Our experiments permit only semi-quantitative conclusions about the efficiency and optimum of each
514 transporter, since we did not assay binding affinity and maximal transport velocity with ^{32}P uptake
515 measurements. Pi uptake experiments in early timepoints are likely not confounded by different growth
516 rates of each triple mutant expressing a single Pi transporter "alone" because all experiments were
517 performed at an OD_{600} of 2. However, inefficient Pi uptake may be artifactually amplified by slower growth
518 of mutants at time points longer than 4-6 hours. Another potential confounder could be differential
519 expression levels of the 4 transporters, which are likely to vary between pH and Pi concentration
520 conditions; e.g. the alkali-responsive transcriptional regulator Rim101 induces transcription of *PHO89*
521 [87], and protein levels of these 4 *C. albicans* transporters remain to be defined. Our in vitro evolution
522 experiment was limited in that 2 transformants from a final strain-construction transformation step were
523 evolved without technical replicates; nevertheless, experimental testing of candidate variants will be
524 required in any case to ascribe fitness roles in Pi scarcity to mutations identified in both or in one of the
525 phenotypically distinct lineages.

526

527 In summary, *C. albicans'* Pi acquisition system is suboptimal for the neutral to alkaline host environments
528 it typically occupies during invasive disease. Differences in functional optima among transporters may
529 provide backup mechanisms for Pi transport as *C. albicans* moves through different host niches.
530 Redistribution of intracellular Pi among organelles and processes may sustain survival during "alkaline pH-
531 simulated nutrient deprivation" [69], in ways that remain to be elucidated. At the same time, this
532 redistribution might also render the fungus more sensitive to host-relevant stressors like membrane- and
533 cell wall stress. Pi acquisition and regulation in humans differs fundamentally from that in fungi; given the
534 crucial role of phosphorus in structural, metabolic and regulatory processes and in antifungal drug
535 endurance, definition of these systems could reveal potential fungus-specific drug targets.

536

537 **Methods**

538

539 **Culture conditions.**

540 Cells were grown in rich complex medium, YPD, defined media synthetic complete (SC) or yeast nitrogen
541 base (YNB) with 2 % glucose as described in [25, 26]. To provide defined Pi concentrations, Yeast Nitrogen
542 Base without Amino Acids, without Ammonium sulphate and without Phosphate, supplemented with KCl,
543 was used (CYN6802, Formedium, Swaffham, Norfolk, England) and supplemented with the indicated
544 concentrations of KH_2PO_4. Incubation temperatures were 30°C for liquid and solid media except for hyphal
545 growth assays which were incubated at 37°C.

546

547 **Strain construction.**

548 *C. albicans* mutants were generated as in [88]; details of strain construction are provided in S2 Table
549 (Strains used in this study), S3 Table (Plasmids used in this study) and S4 Table (Oligonucleotides used in
550 this study). At least 2 and typically 3 independent heterozygous lineages were constructed for each set of
551 deletion mutants. Only during construction of the Q- strain, 2 isolates were generated from a single *pho84-*
552 */- pho89-/- pho87-/- fgr2/FGR2* heterozygous parent. At each mutant construction step, we compared
553 growth phenotypes of independent transformants in synthetic media; isolates with outlier phenotypes
554 were eliminated from further use, since those presumably were due to unrelated mutations that arose
555 during transformation. Among isogenic mutants with similar phenotypes, we performed initial phenotypic
556 characterizations with 2 or more isolates to confirm their similar behaviors. The null mutants for each

557 predicted transporter were used to examine the role of that transporter in filamentous growth, stress
558 responses, susceptibility to antifungal agents and TORC1 signaling.
559
560 **Growth curves**.
561 Cells from glycerol stocks at -80ºC were recovered on YPD agar medium for 2 days. Cells were scraped
562 from the plate and washed twice with NaCl 0.9% and diluted to a final OD_{600} 0.01 in 150 µl medium in flat
563 bottom 96-well plates. OD_{600} readings were obtained every 15 min in a Biotech Synergy 2 Multi-Mode
564 Microplate Reader (Winooski, VT, USA). Standard deviations of three technical replicates, representing
565 separate wells, were calculated, and graphed in Graphpad Prism Version 9.5.1 (528), and displayed as
566 error bars. At least 3 biological replicates were obtained on different days unless stated otherwise. For
567 some assays the area under the curve was calculated and graphed using the same software, and the
568 average from ≥3 biological replicates per condition was graphed.
569
570 **Phosphate uptake.**
571 Phosphate uptake measurement experiments were performed as in [23] with some modifications. In brief,
572 cells were incubated with a defined amount of Pi; the rate of Pi removal from the medium corresponds to
573 the strains' Pi transport capacity. Cells were recovered on YPD plates from glycerol stocks at -80ºC for 2
574 days. SC medium without Pi, buffered at one-unit increments from pH 2 to 8 was inoculated with cells at
575 an OD_{600} of 2. Cells were given 30 minutes to equilibrate, 1 mM Pi was then added, and the Pi remaining
576 in the medium was measured every 1-5 h for a period of 6 to 30 hours, depending on each strain or
577 condition. Samples were harvested at 20,000 rpm for 5 min in the cold room and two technical replicates
578 per sample (300 µl) were collected from each time point. The total concentration of Pi in the supernatant
579 was calculated according to Ames [89].
580
581 When the assay required pre-feeding the cells with GPC before the addition of Pi, 10 mM of GPC was
582 added during the 30-minute incubation without Pi. Then Pi was added at a concentration of 1 mM.
583
584 **Growth of cell dilution spots on solid medium**.
585 Cells recovered from glycerol stock at -80ºC were grown on YPD plates for ≥2 days. They were washed in
586 0.9 % NaCl and diluted in 5- or 3-fold steps from a starting OD_{600} of 0.5 in a microtiter plate, then pin
587 transferred to agar medium and incubated for 48 h at 30°C.

588

589 **Hyphal morphogenesis assay**.

590 Cells recovered from glycerol stock at -80°C were grown on YPD plates for 1-2 days, washed and
591 resuspended in 0.9% NaCl to an OD_{600} 0.1. Variation between spots and spot density effects were
592 minimized by spotting 3 µl cell suspensions at 6 equidistant points, using a template around the perimeter
593 of an agar medium plate. Each agar plate contained a WT spot that served as a control to which the other
594 strains on the plate must be compared. This method minimizes variation between colony filamentation
595 within each genotype that occurs when colonies are streaked or plated at varying density and at
596 uncontrolled distances from each other. By including a WT on each plate, we also control for the effects
597 of different hydration states of the agar and slight variations in medium composition which cannot be
598 excluded by other means. RPMI and Spider media were used; the latter is not buffered and has a slightly
599 higher than neutral pH. RPMI medium pH 7 was buffered with 165 mM MOPS; and RPMI pH 5 was buffered
600 with 100 mM MES. Plates were incubated at 37°C for the indicated durations. All panels shown represent
601 at least 3 biological replicates.

602

603 **Western blot.**

604 Cell lysis and Western blotting were performed as described in [62]. Antibodies used are shown in S5
605 Table. For densitometry, ImageJ (imagej.net/welcome) software (opensource) was used to quantitate
606 signals obtained from Azure biosystems c600.

607

608 **Population evolution.**

609 Two Q- mutants (*pho84-/- pho89-/- pho87-/- fgr2-/-*), distinct transformants (Q- L1 and Q- L2)for deletion
610 of the second *FGR2* allele, derived from the same heterozygous strain (JKC2812 *pho84-/- pho89-/- pho87-*
611 */- fgr2-/FGR2*), were inoculated into 10 ml SC 0.4 mM Pi at an OD_{600} of 0.05. Cultures were incubated at
612 30°C at 200 rpm. From each culture, 10 µl were transferred into 10 ml of the same fresh medium every
613 48 hours, for a total of 30 passages. The culture from each passage was saved as a glycerol stock.
614 Populations from each passage were used in growth curve experiments and were always used after direct
615 revival from frozen stock without further passaging.

616

617 **Genomic DNA isolation and whole-genome sequencing.**

618 For DNA extraction from cells grown on YPD plates from cells saved at the end of each passage, the Zymo
619 Quick DNA Fungal/Bacterial Miniprep kit was used according to the manufacturer's instructions.Library
620 preparation and sequencing was carried out by the Applied Microbiology Services Lab (AMSL) at The Ohio
621 State University, using the Illumina Nextseq 2000 platform to generate 150 basepair paired-end reads. All
622 samples were sequenced to a minimum depth of 175x. The reads were trimmed using trimmomatic 0.39
623 (with default parameters except slidingwindow:4:20, maxinfo:125:1, headcrop:20, and minlen:35) to
624 remove adaptors and poor quality sequences [90]. Using bowtie2 v2.2.6 [91], the trimmed reads were
625 aligned against the SC5314 reference genome (version A21-s02-m09-r10) obtained from the Candida
626 Genome Database (www.candidagenome.org). The aligned SAM files were then converted to the BAM
627 format using samtools v1.7 [92].
628
629 **Copy number analysis.**
630 To detect karyotypic changes, pileup data for each whole-genome sequenced strain was obtained using
631 bbMAP v39.01 [93]. Average read pileup depth highlighted any whole-chromosome aneuploidies. Copy
632 number variation, including aneuploidies, were further confirmed via visualization in YMAP [94].
633
634 **Data availability.**
635 The sequencing data are available at the Sequence Read Archive under BioProject Accession Number
636 PRJNA1035923.
637
638 **Acknowledgements**
639
640 We thank Yuping Li for helpful discussions. M.A.-Z. was funded in part by the Alfonso Martin Escudero
641 Foundation (Madrid, Spain). J.R.K. was funded by Boston Children's Hospital and by NIAID R21AI096054
642 and NIAID R21AI137716. M.Z.A. was funded by National Institutes of Health grant 1R01AI148788 and an
643 NSF CAREER Award 2046863. A.M. was supported by a President's Postdoctoral Scholars Program Award
644 at The Ohio State University. J.P.-V. was funded by NIH R15 GM104876. The funders played no role in the
645 study design, data collection and analysis, decision to publish, or preparation of the manuscript. The
646 authors declare no competing interests, financial or non-financial.
647
648

649 **Table 1. Pi transporter characteristics.**

	Pho84	Pho89	Pho87	Fgr2
Chromosomal location	Chr1	Chr4	Chr1	Chr7
Pi affinity	high	high	low	low
Optimal pH range	pH 2-8	pH 6-8	pH 2-6	pH 3-4
Role in hyphal growth	+++	+	-	-
Role in Target of Rapamycin Complex1 signaling	Yes	No	No	No
Role in oxidative stress response	Yes	No	No	No

650

651

652 **Figure Legends**

653

654 **Fig. 1. Among Pi transporters, Pho84 contributed to growth over the broadest range of tested**
655 **conditions.** Fivefold dilutions of cells of indicated genotypes were spotted (top to bottom) onto YPD (top,
656 center) or SC (all others) agar media buffered to indicated pH (3, 5 or 7) with 100 mM MES and containing
657 indicated Pi concentrations (0.05, 0.5 or 7.3 mM) and grown at 30° C for 2 d. Strains are WT (JKC915);
658 *pho84-/-* (JKC1450); *pho89-/-* (JKC2585); *pho87-/-* (JKC2581); *fgr2-/-* (JKC2667); Pho84-A: *pho87-/- pho89-*
659 */- fgr2-/- PHO84+/+* (JKC2788); Pho89-A: *pho84-/- pho87-/- fgr2-/- PHO89+/+* (JKC2783); Pho87-A: *pho84-*
660 */- pho89-/- fgr2-/- PHO87+/+* (JKC2777); Fgr2-A: *pho84-/- pho87-/- pho89-/- FGR2+/+* (JKC2758); Q-:
661 *pho84-/- pho87-/- pho89-/- fgr2-/-* (JKC2830 and JKC2860). Representative of 3 biological replicates.

662

663 **Fig. 2. Pho84 was the major contributor to hyphal growth among 4 Pi transporters.** Cell suspensions of
664 indicated genotypes were spotted at equidistant points around the perimeter of Spider (**A**) and RPMI (**B,**
665 **C**) agar plates. Photomicrographs of the edge of spots were obtained at 4 days for RPMI and 11 days for
666 Spider plates. Spot edges were aligned with image frame corners to allow comparisons of hyphal fringes'
667 length. Strains are WT (JKC915); *pho84-/-* (JKC1450); Pho84-A: *pho87-/- pho89-/- fgr2-/- PHO84+/+*
668 (JKC2788); *pho89-/-* (JKC2585); Pho89-A: *pho84-/- pho87-/- fgr2-/- PHO89+/+* (JKC2783)*; pho87-/-*
669 (JKC2581); Pho87-A: *pho84-/- pho89-/- fgr2-/- PHO87+/+* (JKC2777); *fgr2-/-* (JKC2667); Fgr2-A: *pho84-/-*
670 *pho87-/- pho89-/- FGR2+/+* (JKC2758); Q- L1: *pho84-/- pho87-/- pho89-/- fgr2-/-* (JKC2830); Q- L2: *pho84-*
671 */- pho87-/- pho89-/- fgr2-/-* (JKC2860). Size bar 200 µm. Representative of 3 biological replicates.

672

673 **Fig. 3. Pho84 was required for TORC1 activation.** Cells were grown in YNB with indicated Pi concentrations
674 for 90 min. Western blots were probed against phosphorylated Rps6 (P-S6) for monitoring TORC1 activity,
675 and tubulin (Tub) as loading control. Dens: ratio between P-S6 and tubulin signals by densitometry.
676 Representative of 3 biological replicates. Strains are 1: WT (JKC915); 2: *pho84-/-* (JKC1450); 3: *pho87-/-*
677 (JKC2581); 4: *pho89-/-* (JKC2585) and 5: *fgr2-/-* (JKC2667)
678
679 **Fig. 4. Pi transporters differed for their optimal pH and Pi concentration range while Pho84 was most**
680 **active overall.** Cells expressing the indicated Pi transporter alone among the 4 Pi transporters were
681 inoculated to an OD_{600} of 0.2 into SC medium buffered to the indicated pH with 100 mM MES and grown
682 in a plate reader at 30° C for 20 h. OD_{600} was measured every 15 min and the area under the growth curve
683 was calculated in Graphpad Prism; means of 3 biological replicates are depicted in histograms. See S3 Fig.
684 for the represented growth curves. Error bars represent SD of 3 biological replicates. **A.** SC containing 0.1
685 mM KH_2PO_4. **B.** SC containing 7.3 mM KH_2PO_4. Strains are WT (JKC915); Pho84-A: *pho87-/- pho89-/- fgr2-*
686 */- PHO84+/+* (JKC2788); Pho87-A: *pho84-/- pho89-/- fgr2-/- PHO87+/+* (JKC2777); Pho89-A: *pho84-/-*
687 *pho87-/- fgr2-/- PHO89+/+* (JKC2783)*;* Fgr2-A: *pho84-/- pho87-/- pho89-/- FGR2+/+* (JKC2758).
688
689 **Fig. 5. Pi uptake of cells expressing single Pi transporters reflected their growth optima.** Cells with
690 indicated genotypes were inoculated into SC without Pi (buffered to pH 1-9) at OD_{600} 2. After 30 minutes,
691 KH_2PO_4 was added to a final concentration of 1 mM, and the extracellular concentration of phosphate was
692 measured in 2 technical replicates at indicated time points. Error bars SD. Representative of three
693 biological replicates. **A.** WT (JKC915). **B.** Pho84-A: *pho87-/-pho89-/- fgr2-/- PHO84+/+* (JKC2788). **C.**
694 Pho89-A in pH 1-5; **D.** Pho89-A in pH 6-9: *pho84-/-pho87-/- fgr2-/- PHO89+/+* (JKC2783). **E.** Pho87-A:
695 *pho84-/-pho89-/- fgr2-/- PHO87+/+* (JKC2777). **F.** Fgr2-A: *pho84-/- pho87-/- pho89-/- FGR2+/+* (JKC2758).
696 **G.** Q- cells (*pho84-/- pho87-/- pho89-/- fgr2-/-;* JKC2830) took up significantly less Pi at pH 4 than Fgr2-A
697 cells at 30 h of incubation. Histograms depict average and SD of 3 biological replicates, p=0.0001 (two-
698 tailed t-test).
699
700 **Fig. 6. Cells lacking 4 Pi transporters showed residual Pi uptake ability that was outcompeted by**
701 **glycerophosphocholine. A.** Pi uptake experiments performed as in Fig. 5 showed that in Q- cells (*pho84-*
702 */- pho87-/- pho89-/- fgr2-/-*, JKC2830) residual Pi uptake occurred and was most efficient at pH 4. **B.**
703 Tenfold excess glycerophosphocholine (GPC) inhibited Pi uptake in Q- cells at pH 4. As in Fig. 5, Q- cells

704 (JKC2830) were inoculated into SC 0 Pi with 10 mM GPC; after 30 minutes, KH_2PO_4 was added to a final
705 concentration of 1 mM; Pi concentration in the medium was measured with 3 technical replicates at each
706 time point. Graph shows mean of 3 biological replicates. Error bars SD. **C.** Cells in which *PHO87* is
707 expressed from repressible *tetO* while the other 3 Pi transporters and *GIT2-4* are deleted (*tetO-*
708 *PHO87/pho87 pho84-/- pho89-/- fgr2-/- git2-4-/-,* JKC2969), grew well in the absence of doxycycline but
709 grew minimally during *tetO* repression in 50 µg/ml doxycycline. WT (JKC915) and *tetO-PHO87* (JKC2969)
710 were starved for Pi in SC 0 Pi in the presence of 50 µg/ml doxycycline for 48 h. The medium and doxycyline
711 were replaced every 24 h. Cells were then inoculated at OD 0.01 into SC medium (7.3 mM Pi), buffered to
712 pH 3 with 100 mM MES, without and with 50 µg/ml Doxycycline. OD_{600} was recorded every 15 min. Error
713 bars SD of 3 technical replicates. Representative of 3 biological replicates.
714
715 **Fig. 7. Whole genome sequencing revealed aneuploidies in Q- cells, and evolution of 2 Q- lineages during**
716 **Pi scarcity proceeded along distinct trajectories. A.** Cells from selected passages of populations evolving
717 under Pi starvation from Q- isolates JKC2830 and JKC2860 were grown in SC 0.4 mM Pi. Representative
718 growth curves and corresponding area under the curve (AUC) shown for selected passages. P0 denotes
719 the Q- isolate before passaging; all experiments after P0 were performed with populations, not with
720 clones derived from single colonies. Growth curves are representative of 3 biological replicates, except for
721 passages 4 and 8, which are representative of 2 biological replicates. Error bars SD of 3 technical replicates.
722 **B**. YMAP [74] depictions of WGS results of 2 distinct Q- isolates (*pho84-/- pho87-/- pho89-/- fgr2-/-* ,
723 JKC2830, Q- L1 and JKC2860, Q- L2) showing Chr5 trisomy and loss of heterozygosity of Chr2 and Chr3.
724
725 **Fig. 8. Whole genome sequencing of selected passages of 2 evolving Q- derived populations showed**
726 **distinct trajectories of acquisition and resolution of aneuploidies and loss of heterozygosity.** YMAP [74]
727 depictions of WGS results of populations evolving from JKC2830, Q- L1 and JKC2860, Q- L2 (both *pho84-/-*
728 *pho87-/- pho89-/- fgr2-/-*).
729
730 **Fig. 9. Two evolving lineages of Q- cells showed distinct stressor endurance. A**. Growth area under the
731 curve (AUC) of cells grown in SC 1 mM Pi containing Vehicle (Veh, DMSO), 0.3 µg/ml Amphotericin B
732 (AmpB) or 0.005% SDS. AmpB representative of 2 and SDS of 3 biological replicates; error bar SD of 3
733 technical replicates. **B**. Amphotericin B (AmpB) and SDS growth area under the curve (AUC) from panel A
734 normalized to each strain's vehicle (Veh) control. WT (JKC915); Q- L1 (JKC2830); Q- L1 P30 (JKC2830

735 passage 30); Q- L2 (JKC2860); Q- L2 P30 (JKC2860 passage 30). AmpB average of 2 and SDS of 3 biological
736 replicates; error bar SD of biological replicates. **C**. Threefold dilutions of cells of indicated genotypes,
737 starting at OD_{600} 0.5, were spotted (top to bottom) onto SC medium containing Vehicle (Veh, H_2O) or 10
738 ng/ml micafungin (Mica), 15 µM plumbagin (Plum), 50 ng/ml rapamycin (Rapa), and grown at 30°C for 1
739 d (Mica), 2 d (Plum), 4 d (Rapa), respectively. Strains are WT (JKC915); Q- L1 (JKC2830) passage 0, 4, 13,
740 19, 30 and Q- L2 (JKC2860) passages 0, 5, 7, 19, 30; *pho84-/-* (JKC1450). JKC2830 and JKC2860 genotypes
741 are *pho84-/- pho87-/- pho89-/- fgr2-/-*.
742
743 **S1 Fig. Structural comparisons of Pho84 and its homologs.** AlphaFold structure prediction of *S. cerevisiae*
744 Pho84 and *C. albicans* Fgr2 was obtained from the AlphaFold Protein Structure Database
745 (https://alphafold.ebi.ac.uk/) and visualized in ChimeraX-1.4. The coloring of each model is based on a
746 per-residue confidence score (pLDDT): dark blue – very high (pLDDT > 90), light blue – confident (90 >
747 pLDDT > 70), yellow – low (70 > pLDDT > 50), orange – very low (pLDDT < 50). Inorganic phosphate
748 transporters were aligned in MacVector; identical amino acid residues tinted with dark gray and
749 chemically similar ones in light gray.
750
751 **S2 Fig. Among Pi transporters, only Pho84 was required for oxidative stress endurance.** Cell suspensions
752 of the indicated genotypes WT JKC915; *pho84-/-* (JKC1450); *pho87-/-* (JKC2581); *pho89-/-* (JKC2585); *fgr2-*
753 */-* (JKC2667) and *git2-4-/-* (JKC2963) were spotted in 3-fold dilution steps onto SC medium with DMSO
754 (Veh) or plumbagin 15 µM. Plates were incubated for 2 days at 30° C. Representative of 3 biological
755 replicates. All spots were on the same plate.
756
757 **S3 Fig. Individual growth curves summarized in Figure 4.** Strains were grown as described in Fig. 4. Shown
758 are 3 biological replicates performed on different days. Error bars SD of 2 or 3 technical replicates. Strains
759 are WT (JKC915); Pho84-A: *pho87-/- pho89-/- fgr2-/- PHO84+/+* (JKC2788); Pho87-A: *pho84-/- pho89-/-*
760 *fgr2-/- PHO87+/+* (JKC2777); Pho89-A: *pho84-/- pho87-/- fgr2-/- PHO89+/+* (JKC2783)*;* Fgr2-A: *pho84-/-*
761 *pho87-/- pho89-/- FGR2+/+* (JKC2758).
762
763 **S4 Fig. Pi transporter triple mutants had no growth defects in rich complex medium.** Cells of indicated
764 triple mutant genotypes were grown in YPD (left) and SC (right) and OD_{600} was monitored. Upper panels:
765 strains expressing only one of 2 high-affinity transporters. Lower panels: Strains expressing only one of 2

766 low-affinity transporters. Pho84-A: *pho87-/- pho89-/- fgr2-/- PHO84+/+* (JKC2788); Pho89-A: *pho84-/-*
767 *pho87-/- fgr2-/- PHO89+/+* (JKC2783); Pho87-A: *pho84-/- pho89-/- fgr2-/- PHO87+/+* (JKC2777); Fgr2-A:
768 *pho84-/- pho87-/- pho89-/- FGR2+/+* (JKC2758). Representative of 3 biological replicates; error bars SD of
769 3 technical replicates.
770
771 **S5 Fig. Cells whose single Pi transporter was expressed from *tetO*, as well as Q- cells and their Pi scarcity-**
772 **evolved descendant populations had no substantial growth defects in rich complex medium.** Strains
773 were grown as in S4 Fig. **A.** Cells in which a single allele of one Pi transporter, *PHO87*, is expressed from
774 repressible *tetO*, were grown in YPD and SC without doxycycline and compared with WT and Q- cells. WT
775 (JKC915), Q- L1 (*pho84-/- pho89-/- pho87-/- fgr2-/-*, JKC2830), *tetO-PHO87* (*tetO-PHO87/pho87 pho84-/-*
776 *pho89-/- fgr2-/- git2-4-/-*, JKC2969). **B.** Growth in YPD of WT (JKC915); Q- L1 (JKC2830) and Q- L2 (*pho84-*
777 */- pho89-/- pho87-/- fgr2-/-*, JKC2860). P30: population from the 30th Pi scarcity passage.
778
779 **References**
780

781 1. Pontes MH, Groisman EA. Protein synthesis controls phosphate homeostasis. Genes &
782 development. 2018;32(1):79-92. Epub 2018/02/14. doi: 10.1101/gad.309245.117. PubMed PMID:
783 29437726; PubMed Central PMCID: PMCPMC5828397.
784 2. Garg A, Sanchez AM, Miele M, Schwer B, Shuman S. Cellular responses to long-term phosphate
785 starvation of fission yeast: Maf1 determines fate choice between quiescence and death associated with
786 aberrant tRNA biogenesis. Nucleic acids research. 2023;51(7):3094-115. Epub 2023/02/17. doi:
787 10.1093/nar/gkad063. PubMed PMID: 36794724; PubMed Central PMCID: PMCPMC10123115.
788 3. Ducousso-Detrez A, Fontaine J, Lounes-Hadj Sahraoui A, Hijri M. Diversity of Phosphate Chemical
789 Forms in Soils and Their Contributions on Soil Microbial Community Structure Changes. Microorganisms.
790 2022;10(3). Epub 2022/03/27. doi: 10.3390/microorganisms10030609. PubMed PMID: 35336184;
791 PubMed Central PMCID: PMCPMC8950675.
792 4. Van Mooy BA, Fredricks HF, Pedler BE, Dyhrman ST, Karl DM, Koblizek M, et al. Phytoplankton in
793 the ocean use non-phosphorus lipids in response to phosphorus scarcity. Nature. 2009;458(7234):69-72.
794 Epub 2009/02/03. doi: 10.1038/nature07659. PubMed PMID: 19182781.
795 5. Oliverio AM, Bissett A, McGuire K, Saltonstall K, Turner BL, Fierer N. The Role of Phosphorus
796 Limitation in Shaping Soil Bacterial Communities and Their Metabolic Capabilities. mBio. 2020;11(5). Epub
797 2020/10/29. doi: 10.1128/mBio.01718-20. PubMed PMID: 33109755; PubMed Central PMCID:
798 PMCPMC7593963.
799 6. Crook M, Swaminathan R. Disorders of plasma phosphate and indications for its measurement.
800 Ann Clin Biochem. 1996;33 (Pt 5):376-96. Epub 1996/09/01. doi: 10.1177/000456329603300502.
801 PubMed PMID: 8888972.
802 7. Muchhal US, Pardo JM, Raghothama KG. Phosphate transporters from the higher plant Arabidopsis
803 thaliana. Proceedings of the National Academy of Sciences of the United States of America.
804 1996;93(19):10519-23. Epub 1996/09/17. doi: 10.1073/pnas.93.19.10519. PubMed PMID: 8927627;
805 PubMed Central PMCID: PMCPMC38418.

806 8. Mitsukawa N, Okumura S, Shirano Y, Sato S, Kato T, Harashima S, et al. Overexpression of an
807 Arabidopsis thaliana high-affinity phosphate transporter gene in tobacco cultured cells enhances cell
808 growth under phosphate-limited conditions. Proceedings of the National Academy of Sciences of the
809 United States of America. 1997;94(13):7098-102. Epub 1997/06/24. doi: 10.1073/pnas.94.13.7098.
810 PubMed PMID: 9192698; PubMed Central PMCID: PMCPMC21291.
811 9. Berndt T, Kumar R. Novel mechanisms in the regulation of phosphorus homeostasis. Physiology
812 (Bethesda). 2009;24:17-25. Epub 2009/02/07. doi: 10.1152/physiol.00034.2008. PubMed PMID:
813 19196648; PubMed Central PMCID: PMCPMC3963411.
814 10. Figueres L, Beck-Cormier S, Beck L, Marks J. The Complexities of Organ Crosstalk in Phosphate
815 Homeostasis: Time to Put Phosphate Sensing Back in the Limelight. Int J Mol Sci. 2021;22(11). Epub
816 2021/06/03. doi: 10.3390/ijms22115701. PubMed PMID: 34071837; PubMed Central PMCID:
817 PMCPMC8199323.
818 11. Persson BL, Petersson J, Fristedt U, Weinander R, Berhe A, Pattison J. Phosphate permeases of
819 Saccharomyces cerevisiae: structure, function and regulation. Biochimica et biophysica acta.
820 1999;1422(3):255-72. Epub 1999/11/05. PubMed PMID: 10548719.
821 12. Nieuwenhuis BJ, Borst-Pauwels GW. Derepression of the high-affinity phosphate uptake in the
822 yeast Saccharomyces cerevisiae. Biochimica et biophysica acta. 1984;770(1):40-6. Epub 1984/02/29. doi:
823 10.1016/0005-2736(84)90071-3. PubMed PMID: 6365165.
824 13. Tamai Y, Toh-e A, Oshima Y. Regulation of inorganic phosphate transport systems in
825 Saccharomyces cerevisiae. Journal of bacteriology. 1985;164(2):964-8. Epub 1985/11/01. doi:
826 10.1128/jb.164.2.964-968.1985. PubMed PMID: 3902805; PubMed Central PMCID: PMCPMC214353.
827 14. Martinez P, Persson BL. Identification, cloning and characterization of a derepressible Na+-coupled
828 phosphate transporter in Saccharomyces cerevisiae. Molecular & general genetics : MGG.
829 1998;258(6):628-38. Epub 1998/07/22. PubMed PMID: 9671031.
830 15. Bun-Ya M, Nishimura M, Harashima S, Oshima Y. The PHO84 gene of Saccharomyces cerevisiae
831 encodes an inorganic phosphate transporter. Molecular and cellular biology. 1991;11(6):3229-38. Epub
832 1991/06/01. PubMed PMID: 2038328; PubMed Central PMCID: PMC360175.
833 16. Berhe A, Fristedt U, Persson BL. Expression and purification of the high-affinity phosphate
834 transporter of Saccharomyces cerevisiae. Eur J Biochem. 1995;227(1-2):566-72. Epub 1995/01/15. doi:
835 10.1111/j.1432-1033.1995.tb20426.x. PubMed PMID: 7851439.
836 17. Saier MH, Reddy VS, Moreno-Hagelsieb G, Hendargo KJ, Zhang Y, Iddamsetty V, et al. The
837 Transporter Classification Database (TCDB): 2021 update. Nucleic acids research. 2021;49(D1):D461-D7.
838 Epub 2020/11/11. doi: 10.1093/nar/gkaa1004. PubMed PMID: 33170213; PubMed Central PMCID:
839 PMCPMC7778945.
840 18. Roomans GM, Blasco F, Borst-Pauwels GW. Cotransport of phosphate and sodium by yeast.
841 Biochimica et biophysica acta. 1977;467(1):65-71. Epub 1977/05/16. doi: 10.1016/0005-2736(77)90242-
842 5. PubMed PMID: 16650.
843 19. Kanehisa M, Furumichi M, Sato Y, Kawashima M, Ishiguro-Watanabe M. KEGG for taxonomy-based
844 analysis of pathways and genomes. Nucleic acids research. 2023;51(D1):D587-D92. Epub 2022/10/28. doi:
845 10.1093/nar/gkac963. PubMed PMID: 36300620; PubMed Central PMCID: PMCPMC9825424.
846 20. Harding SD, Armstrong JF, Faccenda E, Southan C, Alexander SPH, Davenport AP, et al. The
847 IUPHAR/BPS Guide to PHARMACOLOGY in 2024. Nucleic acids research. 2024;52(D1):D1438-D49. Epub
848 2023/10/29. doi: 10.1093/nar/gkad944. PubMed PMID: 37897341; PubMed Central PMCID:
849 PMCPMC10767925.
850 21. Wykoff DD, O'Shea EK. Phosphate transport and sensing in Saccharomyces cerevisiae. Genetics.
851 2001;159(4):1491-9. Epub 2002/01/10. PubMed PMID: 11779791; PubMed Central PMCID: PMC1450841.

852 22. Hurlimann HC, Stadler-Waibel M, Werner TP, Freimoser FM. Pho91 Is a vacuolar phosphate
853 transporter that regulates phosphate and polyphosphate metabolism in Saccharomyces cerevisiae.
854 Molecular biology of the cell. 2007;18(11):4438-45. Epub 2007/09/07. doi: 10.1091/mbc.E07-05-0457.
855 PubMed PMID: 17804816; PubMed Central PMCID: PMC2043573.
856 23. Ghillebert R, Swinnen E, De Snijder P, Smets B, Winderickx J. Differential roles for the low-affinity
857 phosphate transporters Pho87 and Pho90 in Saccharomyces cerevisiae. The Biochemical journal.
858 2011;434(2):243-51. Epub 2010/12/15. doi: 10.1042/BJ20101118. PubMed PMID: 21143198.
859 24. Liu NN, Flanagan PR, Zeng J, Jani NM, Cardenas ME, Moran GP, et al. Phosphate is the third nutrient
860 monitored by TOR in Candida albicans and provides a target for fungal-specific indirect TOR inhibition.
861 Proceedings of the National Academy of Sciences of the United States of America. 2017. Epub 2017/06/02.
862 doi: 10.1073/pnas.1617799114. PubMed PMID: 28566496.
863 25. Liu NN, Uppuluri P, Broggi A, Besold A, Ryman K, Kambara H, et al. Intersection of phosphate
864 transport, oxidative stress and TOR signalling in Candida albicans virulence. PLoS pathogens.
865 2018;14(7):e1007076. Epub 2018/07/31. doi: 10.1371/journal.ppat.1007076. PubMed PMID: 30059535;
866 PubMed Central PMCID: PMCPMC6085062.
867 26. Liu NN, Acosta-Zaldivar M, Qi W, Diray-Arce J, Walker LA, Kottom TJ, et al. Phosphoric Metabolites
868 Link Phosphate Import and Polysaccharide Biosynthesis for Candida albicans Cell Wall Maintenance. mBio.
869 2020;11(2). Epub 2020/03/19. doi: 10.1128/mBio.03225-19. PubMed PMID: 32184254; PubMed Central
870 PMCID: PMCPMC7078483.
871 27. Lamarche MG, Wanner BL, Crepin S, Harel J. The phosphate regulon and bacterial virulence: a
872 regulatory network connecting phosphate homeostasis and pathogenesis. FEMS microbiology reviews.
873 2008;32(3):461-73. Epub 2008/02/06. doi: 10.1111/j.1574-6976.2008.00101.x. PubMed PMID: 18248418.
874 28. Santos-Beneit F. The Pho regulon: a huge regulatory network in bacteria. Frontiers in microbiology.
875 2015;6:402. Epub 2015/05/20. doi: 10.3389/fmicb.2015.00402. PubMed PMID: 25983732; PubMed
876 Central PMCID: PMC4415409.
877 29. Chekabab SM, Harel J, Dozois CM. Interplay between genetic regulation of phosphate homeostasis
878 and bacterial virulence. Virulence. 2014;5(8):786-93. Epub 2014/12/09. doi: 10.4161/viru.29307. PubMed
879 PMID: 25483775; PubMed Central PMCID: PMC4601331.
880 30. Ikeh M, Ahmed Y, Quinn J. Phosphate Acquisition and Virulence in Human Fungal Pathogens.
881 Microorganisms. 2017;5(3). Epub 2017/08/23. doi: 10.3390/microorganisms5030048. PubMed PMID:
882 28829379; PubMed Central PMCID: PMCPMC5620639.
883 31. Elliott SR, Tischler AD. Phosphate Starvation: A Novel Signal that Triggers ESX-5 Secretion in
884 Mycobacterium tuberculosis. Molecular microbiology. 2016. Epub 2016/01/23. doi: 10.1111/mmi.13332.
885 PubMed PMID: 26800324.
886 32. Groschel MI, Sayes F, Simeone R, Majlessi L, Brosch R. ESX secretion systems: mycobacterial
887 evolution to counter host immunity. Nature reviews Microbiology. 2016;14(11):677-91. Epub 2016/09/27.
888 doi: 10.1038/nrmicro.2016.131. PubMed PMID: 27665717.
889 33. Nussaume L, Kanno S, Javot H, Marin E, Pochon N, Ayadi A, et al. Phosphate Import in Plants: Focus
890 on the PHT1 Transporters. Front Plant Sci. 2011;2:83. Epub 2011/01/01. doi: 10.3389/fpls.2011.00083.
891 PubMed PMID: 22645553; PubMed Central PMCID: PMCPMC3355772.
892 34. Auesukaree C, Homma T, Kaneko Y, Harashima S. Transcriptional regulation of phosphate-
893 responsive genes in low-affinity phosphate-transporter-defective mutants in Saccharomyces cerevisiae.
894 Biochemical and biophysical research communications. 2003;306(4):843-50. Epub 2003/06/25. PubMed
895 PMID: 12821119.
896 35. Wykoff DD, Rizvi AH, Raser JM, Margolin B, O'Shea EK. Positive feedback regulates switching of
897 phosphate transporters in S. cerevisiae. Molecular cell. 2007;27(6):1005-13. Epub 2007/09/25. doi:
898 10.1016/j.molcel.2007.07.022. PubMed PMID: 17889672; PubMed Central PMCID: PMC2034509.

36. Fradin C, De Groot P, MacCallum D, Schaller M, Klis F, Odds FC, et al. Granulocytes govern the transcriptional response, morphology and proliferation of Candida albicans in human blood. Molecular microbiology. 2005;56(2):397-415. doi: 10.1111/j.1365-2958.2005.04557.x. PubMed PMID: 15813733.
37. Thewes S, Kretschmar M, Park H, Schaller M, Filler SG, Hube B. In vivo and ex vivo comparative transcriptional profiling of invasive and non-invasive Candida albicans isolates identifies genes associated with tissue invasion. Molecular microbiology. 2007;63(6):1606-28. Epub 2007/03/21. doi: 10.1111/j.1365-2958.2007.05614.x. PubMed PMID: 17367383.
38. Zakikhany K, Naglik JR, Schmidt-Westhausen A, Holland G, Schaller M, Hube B. In vivo transcript profiling of Candida albicans identifies a gene essential for interepithelial dissemination. Cellular microbiology. 2007;9(12):2938-54. Epub 2007/07/25. doi: 10.1111/j.1462-5822.2007.01009.x. PubMed PMID: 17645752.
39. Walker LA, Maccallum DM, Bertram G, Gow NA, Odds FC, Brown AJ. Genome-wide analysis of Candida albicans gene expression patterns during infection of the mammalian kidney. Fungal genetics and biology : FG & B. 2009;46(2):210-9. Epub 2008/11/27. doi: 10.1016/j.fgb.2008.10.012. PubMed PMID: 19032986; PubMed Central PMCID: PMCPMC2698078.
40. Hebecker B, Vlaic S, Conrad T, Bauer M, Brunke S, Kapitan M, et al. Dual-species transcriptional profiling during systemic candidiasis reveals organ-specific host-pathogen interactions. Scientific reports. 2016;6:36055. Epub 2016/11/04. doi: 10.1038/srep36055. PubMed PMID: 27808111; PubMed Central PMCID: PMCPMC5093689.
41. Köhler JR, Acosta-Zaldivar M, Qi W. Phosphate in Virulence of Candida albicans and Candida glabrata. Journal of fungi (Basel, Switzerland). 2020;6(2). Epub 2020/04/01. doi: 10.3390/jof6020040. PubMed PMID: 32224872; PubMed Central PMCID: PMCPMC7344514.
42. Forsburg SL. The art and design of genetic screens: yeast. Nature reviews Genetics. 2001;2(9):659-68. Epub 2001/09/05. doi: 10.1038/35088500. PubMed PMID: 11533715.
43. Ottilie S, Goldgof GM, Calvet CM, Jennings GK, LaMonte G, Schenken J, et al. Rapid Chagas Disease Drug Target Discovery Using Directed Evolution in Drug-Sensitive Yeast. ACS Chem Biol. 2017;12(2):422-34. Epub 2016/12/16. doi: 10.1021/acschembio.6b01037. PubMed PMID: 27977118; PubMed Central PMCID: PMCPMC5649375.
44. Luth MR, Gupta P, Ottilie S, Winzeler EA. Using in Vitro Evolution and Whole Genome Analysis To Discover Next Generation Targets for Antimalarial Drug Discovery. ACS Infect Dis. 2018;4(3):301-14. Epub 2018/02/17. doi: 10.1021/acsinfecdis.7b00276. PubMed PMID: 29451780; PubMed Central PMCID: PMCPMC5848146.
45. Cowell AN, Istvan ES, Lukens AK, Gomez-Lorenzo MG, Vanaerschot M, Sakata-Kato T, et al. Mapping the malaria parasite druggable genome by using in vitro evolution and chemogenomics. Science. 2018;359(6372):191-9. Epub 2018/01/13. doi: 10.1126/science.aan4472. PubMed PMID: 29326268; PubMed Central PMCID: PMCPMC5925756.
46. Antonova-Koch Y, Meister S, Abraham M, Luth MR, Ottilie S, Lukens AK, et al. Open-source discovery of chemical leads for next-generation chemoprotective antimalarials. Science. 2018;362(6419). Epub 2018/12/14. doi: 10.1126/science.aat9446. PubMed PMID: 30523084; PubMed Central PMCID: PMCPMC6516198.
47. Andries K, Verhasselt P, Guillemont J, Gohlmann HW, Neefs JM, Winkler H, et al. A diarylquinoline drug active on the ATP synthase of Mycobacterium tuberculosis. Science. 2005;307(5707):223-7. Epub 2004/12/14. doi: 10.1126/science.1106753. PubMed PMID: 15591164.
48. Selmecki A, Forche A, Berman J. Aneuploidy and isochromosome formation in drug-resistant Candida albicans. Science. 2006;313(5785):367-70. Epub 2006/07/22. doi: 10.1126/science.1128242. PubMed PMID: 16857942; PubMed Central PMCID: PMCPMC1717021.

945 49. Selmecki A, Gerami-Nejad M, Paulson C, Forche A, Berman J. An isochromosome confers drug
946 resistance in vivo by amplification of two genes, ERG11 and TAC1. Molecular microbiology.
947 2008;68(3):624-41. Epub 2008/03/28. doi: 10.1111/j.1365-2958.2008.06176.x. PubMed PMID: 18363649.
948 50. Selmecki AM, Dulmage K, Cowen LE, Anderson JB, Berman J. Acquisition of aneuploidy provides
949 increased fitness during the evolution of antifungal drug resistance. PLoS genetics. 2009;5(10):e1000705.
950 Epub 2009/10/31. doi: 10.1371/journal.pgen.1000705. PubMed PMID: 19876375; PubMed Central
951 PMCID: PMCPMC2760147.
952 51. Huang M, McClellan M, Berman J, Kao KC. Evolutionary dynamics of Candida albicans during in
953 vitro evolution. Eukaryotic cell. 2011;10(11):1413-21. Epub 2011/09/06. doi: 10.1128/EC.05168-11.
954 PubMed PMID: 21890821; PubMed Central PMCID: PMCPMC3209058.
955 52. Carolus H, Pierson S, Munoz JF, Subotic A, Cruz RB, Cuomo CA, et al. Genome-Wide Analysis of
956 Experimentally Evolved Candida auris Reveals Multiple Novel Mechanisms of Multidrug Resistance. mBio.
957 2021;12(2). Epub 2021/04/07. doi: 10.1128/mBio.03333-20. PubMed PMID: 33820824; PubMed Central
958 PMCID: PMCPMC8092288.
959 53. Inglis DO, Arnaud MB, Binkley J, Shah P, Skrzypek MS, Wymore F, et al. The Candida genome
960 database incorporates multiple Candida species: multispecies search and analysis tools with curated gene
961 and protein information for Candida albicans and Candida glabrata. Nucleic acids research.
962 2012;40(Database issue):D667-74. Epub 2011/11/09. doi: 10.1093/nar/gkr945. PubMed PMID: 22064862;
963 PubMed Central PMCID: PMC3245171.
964 54. Uhl MA, Biery M, Craig N, Johnson AD. Haploinsufficiency-based large-scale forward genetic
965 analysis of filamentous growth in the diploid human fungal pathogen C.albicans. The EMBO journal.
966 2003;22(11):2668-78. Epub 2003/05/30. doi: 10.1093/emboj/cdg256. PubMed PMID: 12773383; PubMed
967 Central PMCID: PMC156753.
968 55. Wang JM, Woodruff AL, Dunn MJ, Fillinger RJ, Bennett RJ, Anderson MZ. Intraspecies
969 Transcriptional Profiling Reveals Key Regulators of Candida albicans Pathogenic Traits. mBio. 2021;12(2).
970 Epub 2021/04/22. doi: 10.1128/mBio.00586-21. PubMed PMID: 33879584; PubMed Central PMCID:
971 PMCPMC8092256.
972 56. Shen J, Guo W, Köhler JR. CaNAT1, a heterologous dominant selectable marker for transformation
973 of Candida albicans and other pathogenic Candida species. Infection and immunity. 2005;73(2):1239-42.
974 Epub 2005/01/25. doi: 10.1128/IAI.73.2.1239-1242.2005. PubMed PMID: 15664973; PubMed Central
975 PMCID: PMC547112.
976 57. Lo HJ, Köhler JR, DiDomenico B, Loebenberg D, Cacciapuoti A, Fink GR. Nonfilamentous C. albicans
977 mutants are avirulent. Cell. 1997;90(5):939-49. Epub 1997/09/23. PubMed PMID: 9298905.
978 58. Uppuluri P, Chaturvedi AK, Jani N, Pukkila-Worley R, Monteagudo C, Mylonakis E, et al. Physiologic
979 expression of the Candida albicans pescadillo homolog is required for virulence in a murine model of
980 hematogenously disseminated candidiasis. Eukaryotic cell. 2012;11(12):1552-6. Epub 2012/10/30. doi:
981 10.1128/EC.00171-12. PubMed PMID: 23104566; PubMed Central PMCID: PMC3536276.
982 59. Wang Y, Zhou J, Zou Y, Chen X, Liu L, Qi W, et al. Fungal commensalism modulated by a dual-action
983 phosphate transceptor. Cell Rep. 2022;38(4):110293. Epub 2022/01/27. doi:
984 10.1016/j.celrep.2021.110293. PubMed PMID: 35081357.
985 60. Qi W, Acosta-Zaldivar M, Flanagan PR, Liu NN, Jani N, Fierro JF, et al. Stress- and metabolic
986 responses of Candida albicans require Tor1 kinase N-terminal HEAT repeats. PLoS pathogens.
987 2022;18(6):e1010089. Epub 2022/06/11. doi: 10.1371/journal.ppat.1010089. PubMed PMID: 35687592;
988 PubMed Central PMCID: PMCPMC9223334.
989 61. Ikeh MA, Kastora SL, Day AM, Herrero-de-Dios CM, Tarrant E, Waldron KJ, et al. Pho4 mediates
990 phosphate acquisition in Candida albicans and is vital for stress resistance and metal homeostasis.

991 Molecular biology of the cell. 2016. Epub 2016/07/08. doi: 10.1091/mbc.E16-05-0266. PubMed PMID:
992 27385340.
993 62. Chowdhury T, Köhler JR. Ribosomal protein S6 phosphorylation is controlled by TOR and
994 modulated by PKA in Candida albicans. Molecular microbiology. 2015;98(2):384-402. Epub 2015/07/16.
995 doi: 10.1111/mmi.13130. PubMed PMID: 26173379; PubMed Central PMCID: PMC4631378.
996 63. Bishop AC, Ganguly S, Solis NV, Cooley BM, Jensen-Seaman MI, Filler SG, et al.
997 Glycerophosphocholine utilization by Candida albicans: role of the Git3 transporter in virulence. The
998 Journal of biological chemistry. 2013;288(47):33939-52. Epub 2013/10/12. doi:
999 10.1074/jbc.M113.505735. PubMed PMID: 24114876; PubMed Central PMCID: PMCPMC3837134.
1000 64. Bishop AC, Sun T, Johnson ME, Bruno VM, Patton-Vogt J. Robust utilization of phospholipase-
1001 generated metabolites, glycerophosphodiesters, by Candida albicans: role of the CaGit1 permease.
1002 Eukaryotic cell. 2011;10(12):1618-27. Epub 2011/10/11. doi: 10.1128/EC.05160-11. PubMed PMID:
1003 21984707; PubMed Central PMCID: PMCPMC3232722.
1004 65. Riekhof WR, Naik S, Bertrand H, Benning C, Voelker DR. Phosphate starvation in fungi induces the
1005 replacement of phosphatidylcholine with the phosphorus-free betaine lipid diacylglyceryl-N,N,N-
1006 trimethylhomoserine. Eukaryotic cell. 2014;13(6):749-57. Epub 2014/04/15. doi: 10.1128/EC.00004-14.
1007 PubMed PMID: 24728191; PubMed Central PMCID: PMCPMC4054272.
1008 66. Kretschmer M, Reiner E, Hu G, Tam N, Oliveira DL, Caza M, et al. Defects in phosphate acquisition
1009 and storage influence virulence of Cryptococcus neoformans. Infection and immunity. 2014;82(7):2697-
1010 712. Epub 2014/04/09. doi: 10.1128/IAI.01607-14. PubMed PMID: 24711572; PubMed Central PMCID:
1011 PMC4097646.
1012 67. Couce A, Tenaillon OA. The rule of declining adaptability in microbial evolution experiments. Front
1013 Genet. 2015;6:99. Epub 2015/03/31. doi: 10.3389/fgene.2015.00099. PubMed PMID: 25815007; PubMed
1014 Central PMCID: PMCPMC4356158.
1015 68. Kryazhimskiy S, Rice DP, Jerison ER, Desai MM. Microbial evolution. Global epistasis makes
1016 adaptation predictable despite sequence-level stochasticity. Science. 2014;344(6191):1519-22. Epub
1017 2014/06/28. doi: 10.1126/science.1250939. PubMed PMID: 24970088; PubMed Central PMCID:
1018 PMCPMC4314286.
1019 69. Lev S, Djordjevic JT. Why is a functional PHO pathway required by fungal pathogens to disseminate
1020 within a phosphate-rich host: A paradox explained by alkaline pH-simulated nutrient deprivation and
1021 expanded PHO pathway function. PLoS pathogens. 2018;14(6):e1007021. Epub 2018/06/22. doi:
1022 10.1371/journal.ppat.1007021. PubMed PMID: 29928051; PubMed Central PMCID: PMCPMC6013017.
1023 70. He BZ, Zhou X, O'Shea EK. Evolution of reduced co-activator dependence led to target expansion
1024 of a starvation response pathway. eLife. 2017;6. Epub 2017/05/10. doi: 10.7554/eLife.25157. PubMed
1025 PMID: 28485712; PubMed Central PMCID: PMCPMC5446240.
1026 71. Bhalla K, Qu X, Kretschmer M, Kronstad JW. The phosphate language of fungi. Trends in
1027 microbiology. 2022;30(4):338-49. Epub 2021/09/05. doi: 10.1016/j.tim.2021.08.002. PubMed PMID:
1028 34479774; PubMed Central PMCID: PMCPMC8882699.
1029 72. Lacerda-Abreu MA, Dick CF, Meyer-Fernandes JR. The Role of Inorganic Phosphate Transporters in
1030 Highly Proliferative Cells: From Protozoan Parasites to Cancer Cells. Membranes (Basel). 2022;13(1). Epub
1031 2023/01/22. doi: 10.3390/membranes13010042. PubMed PMID: 36676849; PubMed Central PMCID:
1032 PMCPMC9860751.
1033 73. King WR, Acosta-Zaldivar M, Qi W, Cherico N, Cooke L, Kohler JR, et al. Glycerophosphocholine
1034 provision rescues Candida albicans growth and signaling phenotypes associated with phosphate
1035 limitation. mSphere. 2023:e0023123. Epub 2023/10/16. doi: 10.1128/msphere.00231-23. PubMed PMID:
1036 37843297.

1037 74. Cutler NS, Pan X, Heitman J, Cardenas ME. The TOR signal transduction cascade controls cellular
1038 differentiation in response to nutrients. Molecular biology of the cell. 2001;12(12):4103-13. Epub
1039 2001/12/12. PubMed PMID: 11739804; PubMed Central PMCID: PMC60779.
1040 75. Anderson MZ, Saha A, Haseeb A, Bennett RJ. A chromosome 4 trisomy contributes to increased
1041 fluconazole resistance in a clinical isolate of Candida albicans. Microbiology (Reading). 2017;163(6):856-
1042 65. Epub 2017/06/24. doi: 10.1099/mic.0.000478. PubMed PMID: 28640746; PubMed Central PMCID:
1043 PMCPMC5737213.
1044 76. Yang F, Gritsenko V, Slor Futterman Y, Gao L, Zhen C, Lu H, et al. Tunicamycin Potentiates
1045 Antifungal Drug Tolerance via Aneuploidy in Candida albicans. mBio. 2021;12(4):e0227221. Epub
1046 2021/09/02. doi: 10.1128/mBio.02272-21. PubMed PMID: 34465026; PubMed Central PMCID:
1047 PMCPMC8406271.
1048 77. Bennett RJ, Forche A, Berman J. Rapid mechanisms for generating genome diversity: whole ploidy
1049 shifts, aneuploidy, and loss of heterozygosity. Cold Spring Harbor perspectives in medicine. 2014;4(10).
1050 Epub 2014/08/02. doi: 10.1101/cshperspect.a019604. PubMed PMID: 25081629; PubMed Central PMCID:
1051 PMCPMC4200206.
1052 78. Torres EM, Sokolsky T, Tucker CM, Chan LY, Boselli M, Dunham MJ, et al. Effects of aneuploidy on
1053 cellular physiology and cell division in haploid yeast. Science. 2007;317(5840):916-24. Epub 2007/08/19.
1054 doi: 10.1126/science.1142210. PubMed PMID: 17702937.
1055 79. Ene IV, Farrer RA, Hirakawa MP, Agwamba K, Cuomo CA, Bennett RJ. Global analysis of mutations
1056 driving microevolution of a heterozygous diploid fungal pathogen. Proceedings of the National Academy
1057 of Sciences of the United States of America. 2018;115(37):E8688-E97. Epub 2018/08/29. doi:
1058 10.1073/pnas.1806002115. PubMed PMID: 30150418; PubMed Central PMCID: PMCPMC6140516.
1059 80. Zhu YO, Siegal ML, Hall DW, Petrov DA. Precise estimates of mutation rate and spectrum in yeast.
1060 Proceedings of the National Academy of Sciences of the United States of America. 2014;111(22):E2310-8.
1061 Epub 2014/05/23. doi: 10.1073/pnas.1323011111. PubMed PMID: 24847077; PubMed Central PMCID:
1062 PMCPMC4050626.
1063 81. Yona AH, Manor YS, Herbst RH, Romano GH, Mitchell A, Kupiec M, et al. Chromosomal duplication
1064 is a transient evolutionary solution to stress. Proceedings of the National Academy of Sciences of the
1065 United States of America. 2012;109(51):21010-5. Epub 2012/12/01. doi: 10.1073/pnas.1211150109.
1066 PubMed PMID: 23197825; PubMed Central PMCID: PMCPMC3529009.
1067 82. Tang YC, Amon A. Gene copy-number alterations: a cost-benefit analysis. Cell. 2013;152(3):394-
1068 405. Epub 2013/02/05. doi: 10.1016/j.cell.2012.11.043. PubMed PMID: 23374337; PubMed Central
1069 PMCID: PMCPMC3641674.
1070 83. Yang F, Todd RT, Selmecki A, Jiang YY, Cao YB, Berman J. The fitness costs and benefits of trisomy
1071 of each Candida albicans chromosome. Genetics. 2021;218(2). Epub 2021/04/11. doi:
1072 10.1093/genetics/iyab056. PubMed PMID: 33837402; PubMed Central PMCID: PMCPMC8225349.
1073 84. Coste A, Turner V, Ischer F, Morschhauser J, Forche A, Selmecki A, et al. A mutation in Tac1p, a
1074 transcription factor regulating CDR1 and CDR2, is coupled with loss of heterozygosity at chromosome 5 to
1075 mediate antifungal resistance in Candida albicans. Genetics. 2006;172(4):2139-56. Epub 2006/02/03. doi:
1076 10.1534/genetics.105.054767. PubMed PMID: 16452151; PubMed Central PMCID: PMCPMC1456413.
1077 85. Van Mooy BA, Rocap G, Fredricks HF, Evans CT, Devol AH. Sulfolipids dramatically decrease
1078 phosphorus demand by picocyanobacteria in oligotrophic marine environments. Proceedings of the
1079 National Academy of Sciences of the United States of America. 2006;103(23):8607-12. Epub 2006/05/30.
1080 doi: 10.1073/pnas.0600540103. PubMed PMID: 16731626; PubMed Central PMCID: PMCPMC1482627.
1081 86. Lev S, Rupasinghe T, Desmarini D, Kaufman-Francis K, Sorrell TC, Roessner U, et al. The PHO
1082 signaling pathway directs lipid remodeling in Cryptococcus neoformans via DGTS synthase to recycle

1083 phosphate during phosphate deficiency. PloS one. 2019;14(2):e0212651. Epub 2019/02/23. doi:
1084 10.1371/journal.pone.0212651. PubMed PMID: 30789965; PubMed Central PMCID: PMCPMC6383925.
1085 87. Bensen ES, Martin SJ, Li M, Berman J, Davis DA. Transcriptional profiling in Candida albicans reveals
1086 new adaptive responses to extracellular pH and functions for Rim101p. Molecular microbiology.
1087 2004;54(5):1335-51. Epub 2004/11/24. doi: 10.1111/j.1365-2958.2004.04350.x. PubMed PMID:
1088 15554973.
1089 88. Shen J, Cowen LE, Griffin AM, Chan L, Köhler JR. The Candida albicans pescadillo homolog is
1090 required for normal hypha-to-yeast morphogenesis and yeast proliferation. Proceedings of the National
1091 Academy of Sciences of the United States of America. 2008;105(52):20918-23. Epub 2008/12/17. doi:
1092 10.1073/pnas.0809147105. PubMed PMID: 19075239; PubMed Central PMCID: PMC2634893.
1093 89. Ames BN. Assay of inorganic phosphate, total phosphate and phosphatases. Methods Enzymol.
1094 1966;8:115-8.
1095 90. Bolger AM, Lohse M, Usadel B. Trimmomatic: a flexible trimmer for Illumina sequence data.
1096 Bioinformatics. 2014;30(15):2114-20. Epub 2014/04/04. doi: 10.1093/bioinformatics/btu170. PubMed
1097 PMID: 24695404; PubMed Central PMCID: PMCPMC4103590.
1098 91. Langmead B, Salzberg SL. Fast gapped-read alignment with Bowtie 2. Nature methods.
1099 2012;9(4):357-9. Epub 2012/03/06. doi: 10.1038/nmeth.1923. PubMed PMID: 22388286; PubMed Central
1100 PMCID: PMCPMC3322381.
1101 92. Li H, Handsaker B, Wysoker A, Fennell T, Ruan J, Homer N, et al. The Sequence Alignment/Map
1102 format and SAMtools. Bioinformatics. 2009;25(16):2078-9. Epub 2009/06/10. doi:
1103 10.1093/bioinformatics/btp352. PubMed PMID: 19505943; PubMed Central PMCID: PMCPMC2723002.
1104 93. Bushnell B. BBMap. Available from: sourceforge.net/projects/bbmap/.
1105 94. Abbey DA, Funt J, Lurie-Weinberger MN, Thompson DA, Regev A, Myers CL, et al. YMAP: a pipeline
1106 for visualization of copy number variation and loss of heterozygosity in eukaryotic pathogens. Genome
1107 Med. 2014;6(11):100. Epub 2014/12/17. doi: 10.1186/s13073-014-0100-8. PubMed PMID: 25505934;
1108 PubMed Central PMCID: PMCPMC4263066.
1109

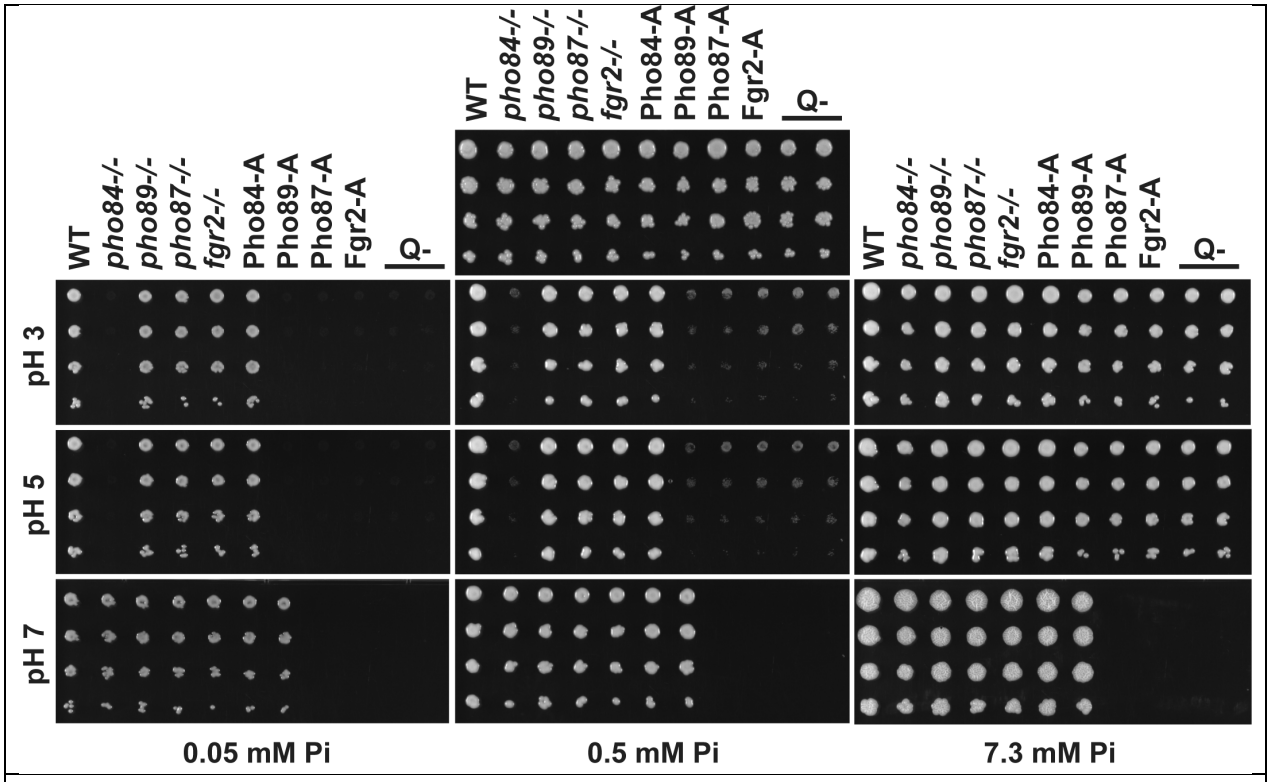

Fig. 1. Among Pi transporters, Pho84 contributed to growth over the broadest range of tested conditions. Fivefold dilutions of cells of indicated genotypes were spotted (top to bottom) onto YPD (top, center) or SC (all others) agar media buffered to indicated pH (3, 5 or 7) with 100 mM MES and containing indicated Pi concentrations (0.05, 0.5 or 7.3 mM) and grown at 30° C for 2 d. Strains are WT (JKC915); *pho84-/-* (JKC1450); *pho89-/-* (JKC2585); *pho87-/-* (JKC2581); *fgr2-/-* (JKC2667); Pho84-A: *pho87-/- pho89-/- fgr2-/- PHO84+/+* (JKC2788); Pho89-A: *pho84-/- pho87-/- fgr2-/- PHO89+/+* (JKC2783); Pho87-A: *pho84-/- pho89-/- fgr2-/- PHO87+/+* (JKC2777); Fgr2-A: *pho84-/- pho87-/- pho89-/- FGR2+/+* (JKC2758); Q-: *pho84-/- pho87-/- pho89-/- fgr2-/-* (JKC2830 and JKC2860). Representative of 3 biological replicates.

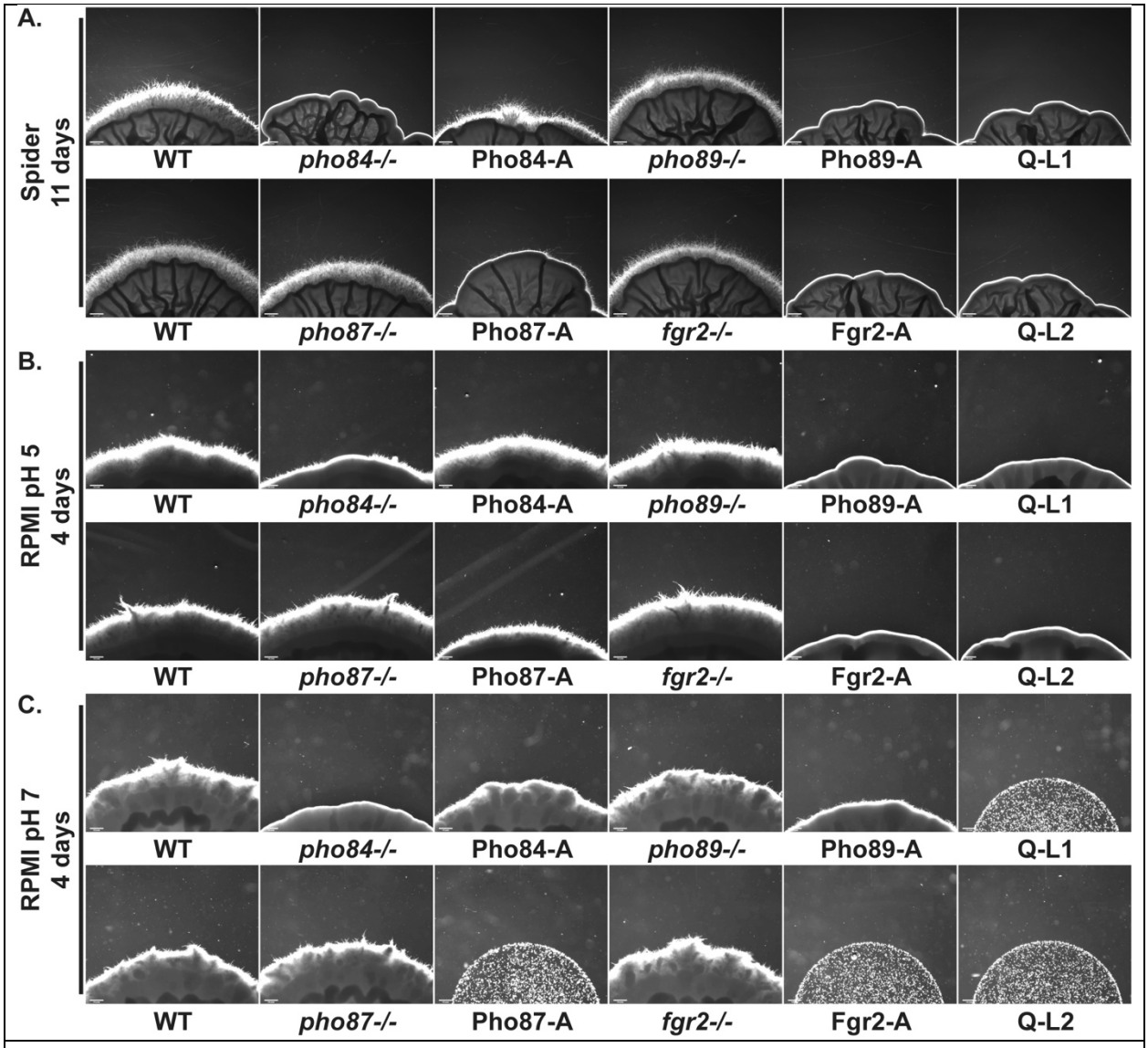

Fig. 2. Pho84 was the major contributor to hyphal growth among 4 Pi transporters. Cell suspensions of indicated genotypes were spotted at equidistant points around the perimeter of Spider (**A**) and RPMI (**B, C**) agar plates. Photomicrographs of the edge of spots were obtained at 4 days for RPMI and 11 days for Spider plates. Spot edges were aligned with image frame corners to allow comparisons of hyphal fringes' length. Strains are WT (JKC915); *pho84-/-* (JKC1450); Pho84-A: *pho87-/- pho89-/- fgr2-/- PHO84+/+* (JKC2788); *pho89-/-* (JKC2585); Pho89-A: *pho84-/- pho87-/- fgr2-/- PHO89+/+* (JKC2783)*; pho87-/-* (JKC2581); Pho87-A: *pho84-/- pho89-/- fgr2-/- PHO87+/+* (JKC2777); *fgr2-/-* (JKC2667); Fgr2-A: *pho84-/- pho87-/- pho89-/- FGR2+/+* (JKC2758); Q-L1: *pho84-/- pho87-/- pho89-/- fgr2-/-* (JKC2830); Q-L2: *pho84-/- pho87-/- pho89-/- fgr2-/-* (JKC2860). Size bar 200 µm. Representative of 3 biological replicates.

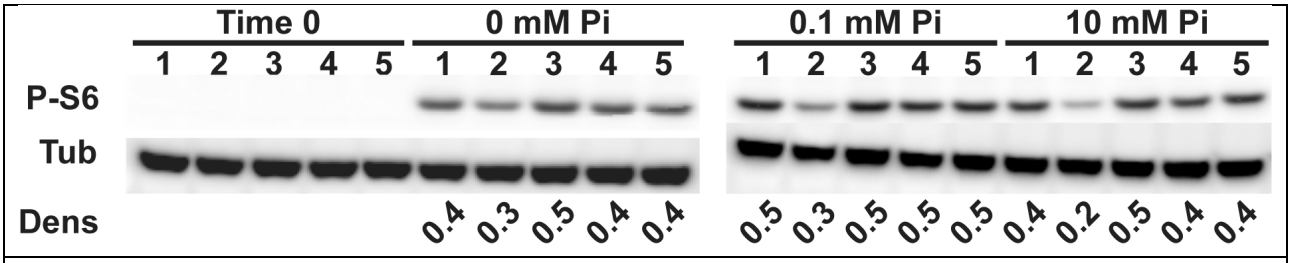

Fig. 3. Pho84 was required for TORC1 activation. Cells were grown in YNB with indicated Pi concentrations for 90 min. Western blots were probed against phosphorylated Rps6 (P-S6) for monitoring TORC1 activity, and tubulin (Tub) as loading control. Dens: ratio between P-S6 and tubulin signals by densitometry. Representative of 3 biological replicates. Strains are 1: WT (JKC915); 2: *pho84-/-* (JKC1450); 3: *pho87-/-* (JKC2581); 4: *pho89-/-* (JKC2585) and 5: *fgr2-/-* (JKC2667)

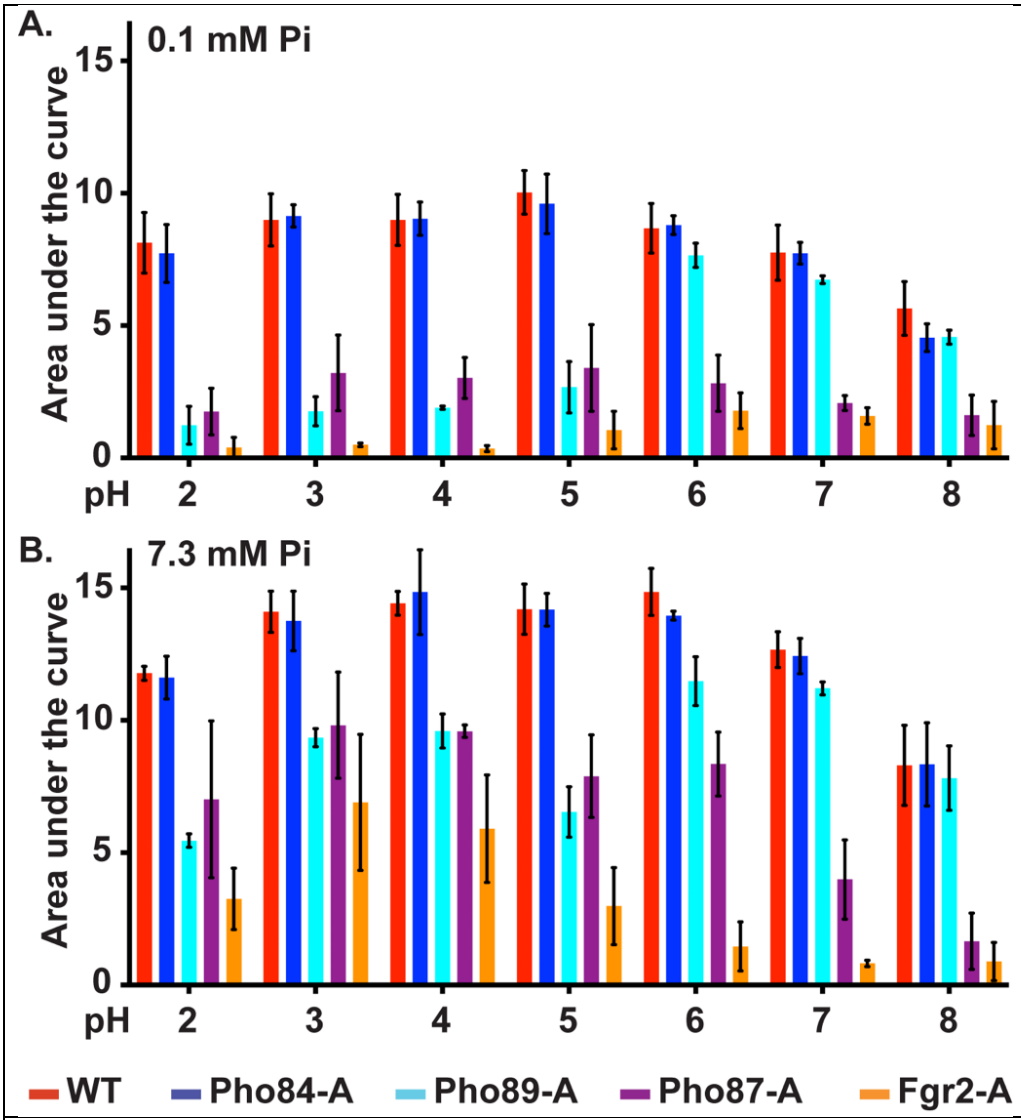

Fig. 4. Pi transporters differed for their optimal pH and Pi concentration range while Pho84 was most active overall. Cells expressing the indicated Pi transporter alone among the 4 Pi transporters were inoculated to an OD_{600} of 0.2 into SC medium buffered to the indicated pH with 100 mM MES and grown in a plate reader at 30° C for 20 h. OD_{600} was measured every 15 min and the area under the growth curve was calculated in Graphpad Prism; means of 3 biological replicates are depicted in histograms. See S3 Fig. for the represented growth curves. Error bars represent SD of 3 biological replicates. **A.** SC containing 0.1 mM KH_2PO_4. **B.** SC containing 7.3 mM KH_2PO_4. Strains are WT (JKC915); Pho84-A: *pho87-/- pho89-/- fgr2-/- PHO84+/+* (JKC2788); Pho87-A: *pho84-/- pho89-/- fgr2-/- PHO87+/+* (JKC2777); Pho89-A: *pho84-/- pho87-/- fgr2-/- PHO89+/+* (JKC2783); Fgr2-A: *pho84-/- pho87-/- pho89-/- FGR2+/+* (JKC2758).

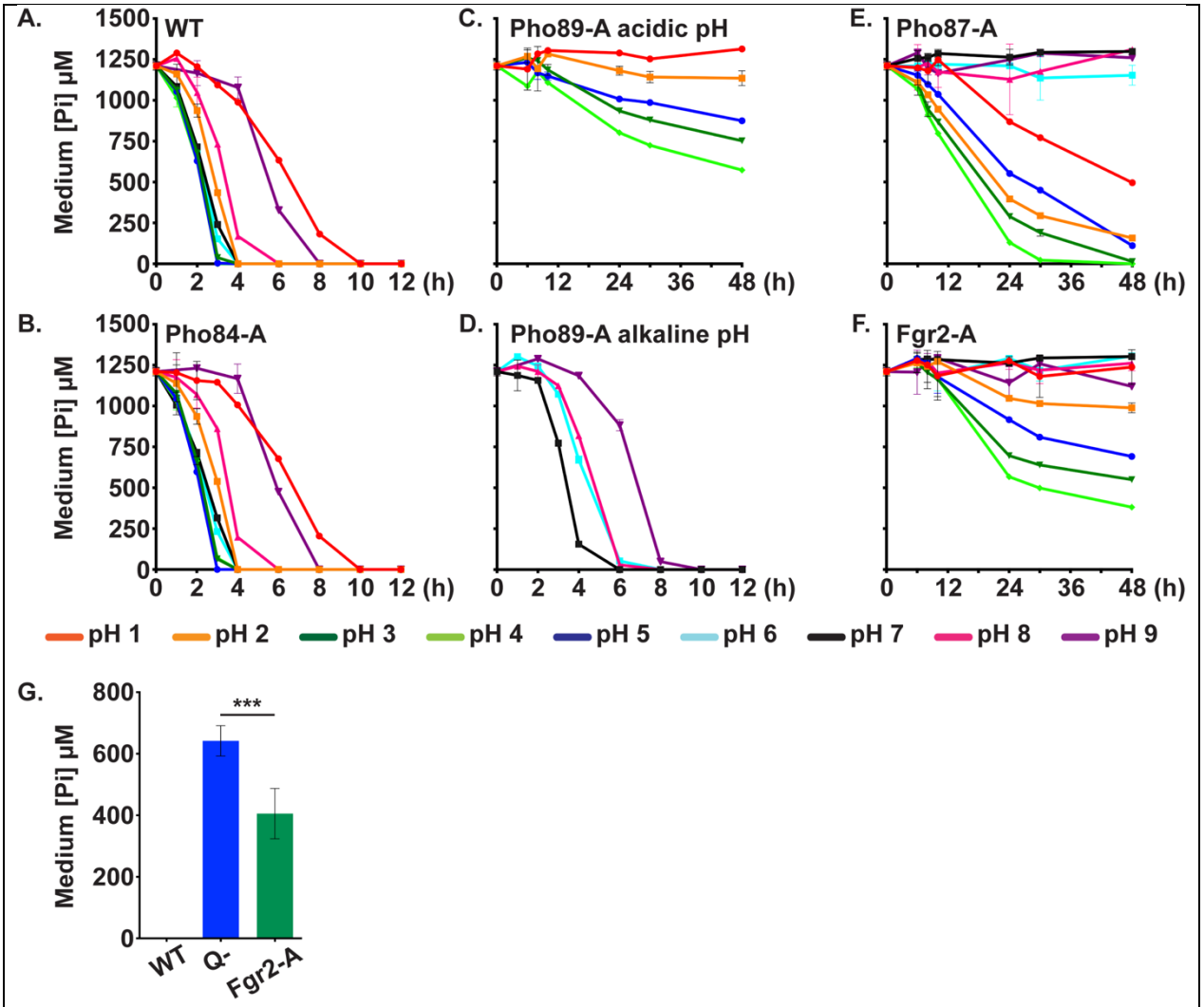

Fig. 5. Pi uptake of cells expressing single Pi transporters reflected their growth optima. Cells with indicated genotypes were inoculated into SC without Pi (buffered to pH 1-9) at OD_{600} 2. After 30 minutes, KH_2PO_4 was added to a final concentration of 1 mM, and the extracellular concentration of phosphate was measured in 2 technical replicates at indicated time points. Error bars SD. Representative of three biological replicates. **A.** WT (JKC915). **B.** Pho84-A: *pho87-/-pho89-/- fgr2-/- PHO84+/+* (JKC2788). **C.** Pho89-A in pH 1-5; **D.** Pho89-A in pH 6-9: *pho84-/- pho87-/- fgr2-/- PHO89+/+* (JKC2783). **E.** Pho87-A: *pho84-/-pho89-/- fgr2-/- PHO87+/+* (JKC2777). **F.** Fgr2-A: *pho84-/- pho87-/- pho89-/- FGR2+/+* (JKC2758). **G.** Q- cells (*pho84-/- pho87-/- pho89-/- fgr2-/-;* JKC2830) took up significantly less Pi at pH 4 than Fgr2-A cells at 30 h of incubation. Histograms depict average and SD of 3 biological replicates, *p*=0.0001 (two-tailed t-test).

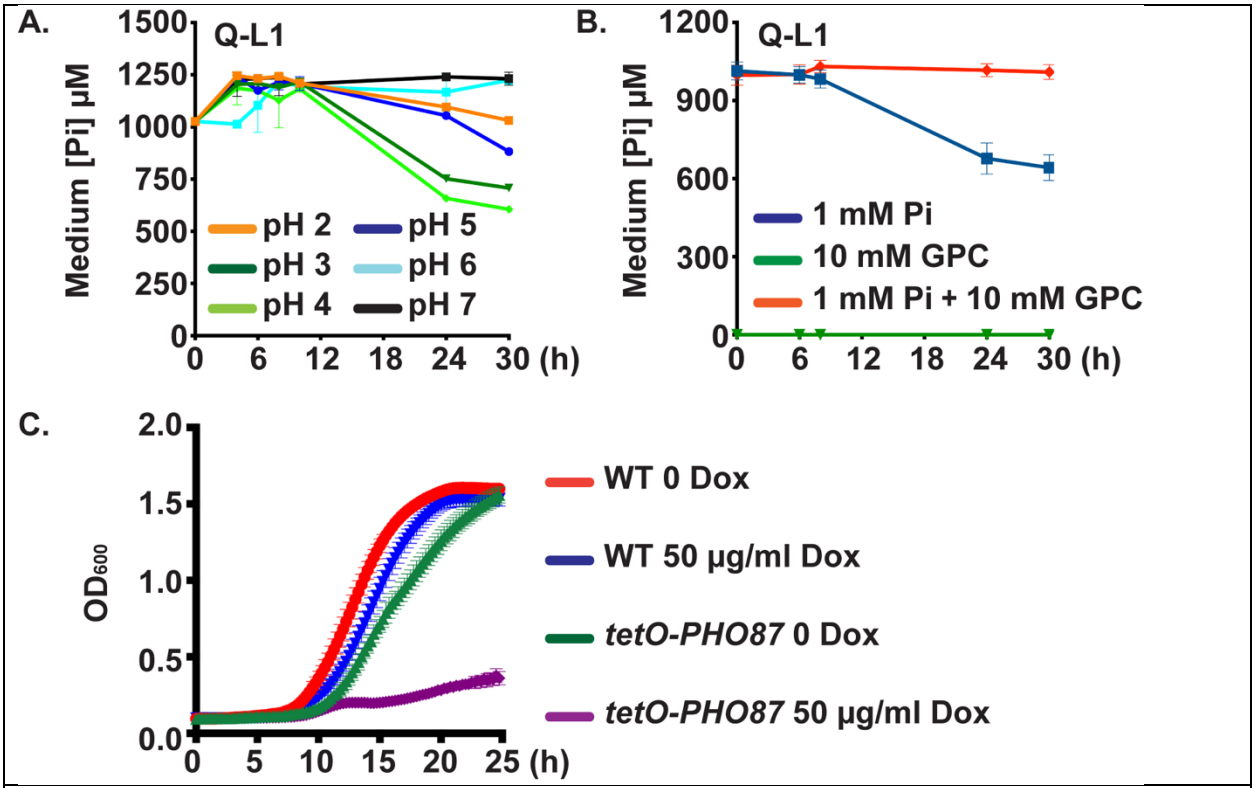

Fig. 6. Cells lacking 4 Pi transporters showed residual Pi uptake ability that was outcompeted by glycerophosphocholine. A. Pi uptake experiments performed as in Fig. 5 showed that in Q- cells (*pho84-/- pho87-/- pho89-/- fgr2-/-*, JKC2830) residual Pi uptake occurred and was most efficient at pH 4. **B.** Tenfold excess glycerophosphocholine (GPC) inhibited Pi uptake in Q- cells at pH 4. As in Fig. 5, Q- cells (JKC2830) were inoculated into SC 0 Pi with 10 mM GPC; after 30 minutes, KH_2PO_4 was added to a final concentration of 1 mM; Pi concentration in the medium was measured with 3 technical replicates at each time point. Graph shows mean of 3 biological replicates. Error bars SD. **C.** Cells in which *PHO87* is expressed from repressible *tetO* while the other 3 Pi transporters and *GIT2-4* are deleted (*tetO-PHO87/pho87 pho84-/- pho89-/- fgr2-/- git2-4-/-,* JKC2969), grew well in the absence of doxycycline but grew minimally during *tetO* repression in 50 µg/ml doxycycline. WT (JKC915) and *tetO-PHO87* (JKC2969) were starved for Pi in SC 0 Pi in the presence of 50 µg/ml doxycycline for 48 h. The medium and doxycyline were replaced every 24 h. Cells were then inoculated at OD 0.01 into SC medium (7.3 mM Pi), buffered to pH 3 with 100 mM MES, without and with 50 µg/ml Doxycycline. OD_{600} was recorded every 15 min. Error bars SD of 3 technical replicates. Representative of 3 biological replicates.

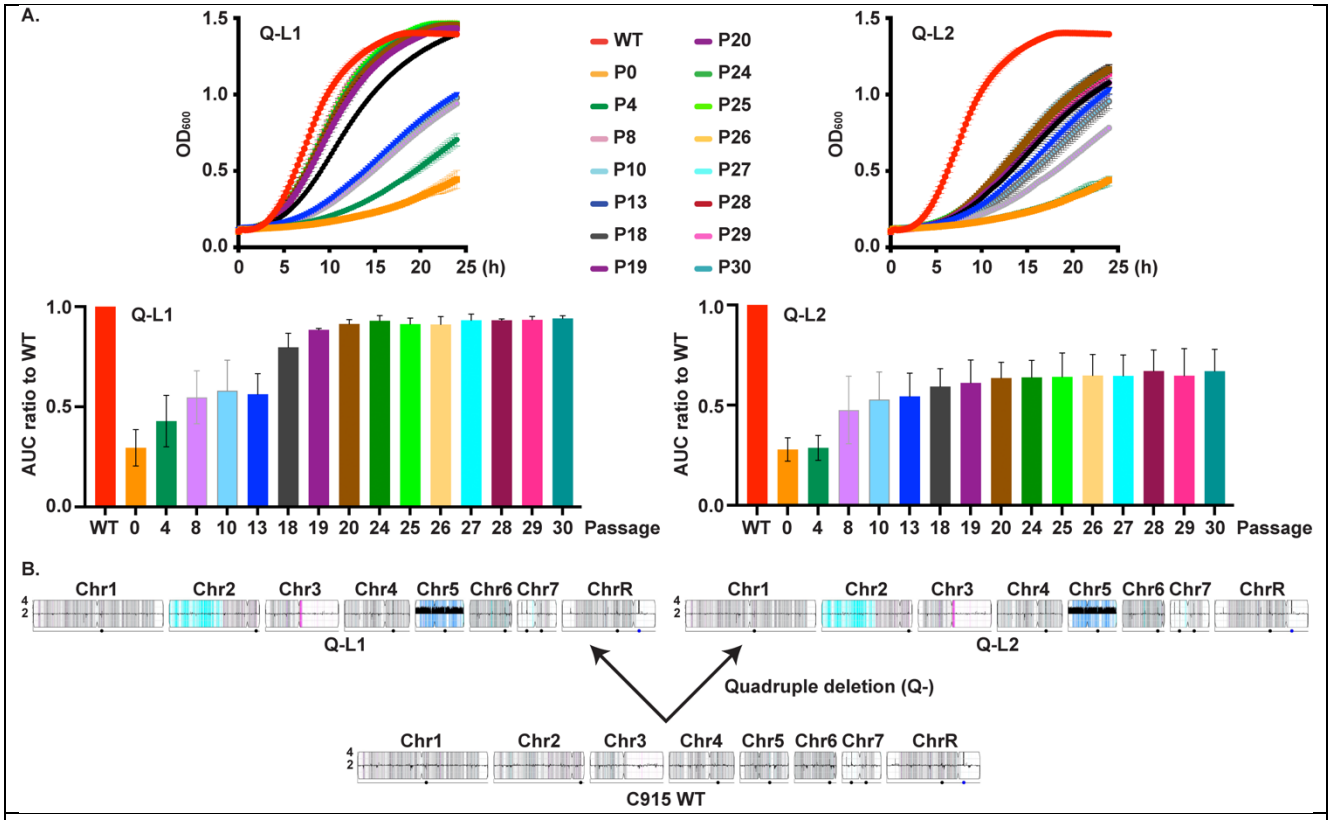

Fig. 7. Whole genome sequencing revealed aneuploidies in Q- cells, and evolution of 2 Q- lineages during Pi scarcity proceeded along distinct trajectories. A. Cells from selected passages of populations evolving under Pi starvation from Q- isolates JKC2830 and JKC2860 were grown in SC 0.4 mM Pi. Representative growth curves and corresponding area under the curve (AUC) shown for selected passages. P0 denotes the Q- isolate before passaging; all experiments after P0 were performed with populations, not with clones derived from single colonies. Growth curves are representative of 3 biological replicates, except for passages 4 and 8, which are representative of 2 biological replicates. Error bars SD of 3 technical replicates. **B**. YMAP [74] depictions of WGS results of 2 distinct Q- isolates (*pho84-/- pho87-/- pho89-/- fgr2-/-* , JKC2830, Q-L1 and JKC2860, Q-L2) showing Chr5 trisomy and loss of heterozygosity of Chr2 and Chr3.

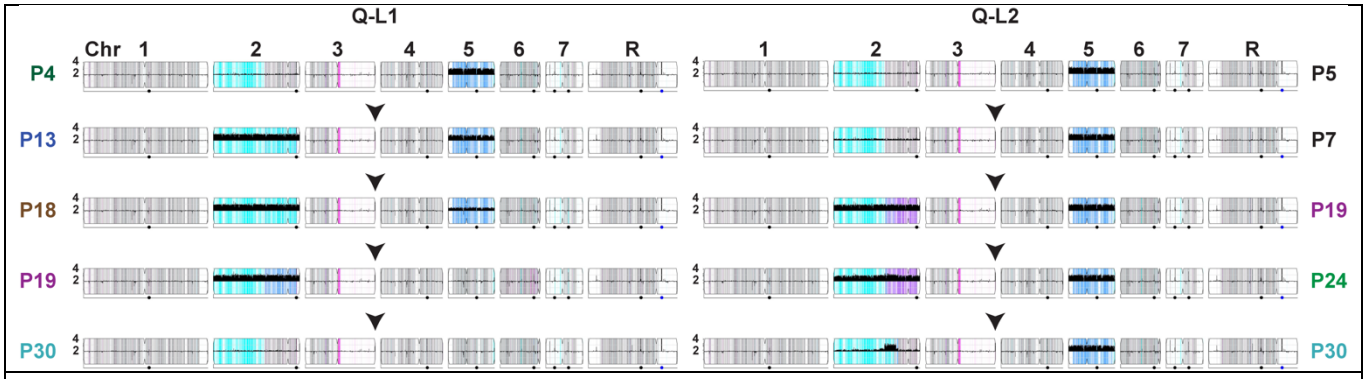

Fig. 8. Whole genome sequencing of selected passages of 2 evolving Q- derived populations showed distinct trajectories of acquisition and resolution of aneuploidies and loss of heterozygosity. YMAP [74] depictions of WGS results of populations evolving from JKC2830, Q-L1 and JKC2860, Q-L2 (both *pho84-/- pho87-/- pho89-/- fgr2-/-*).

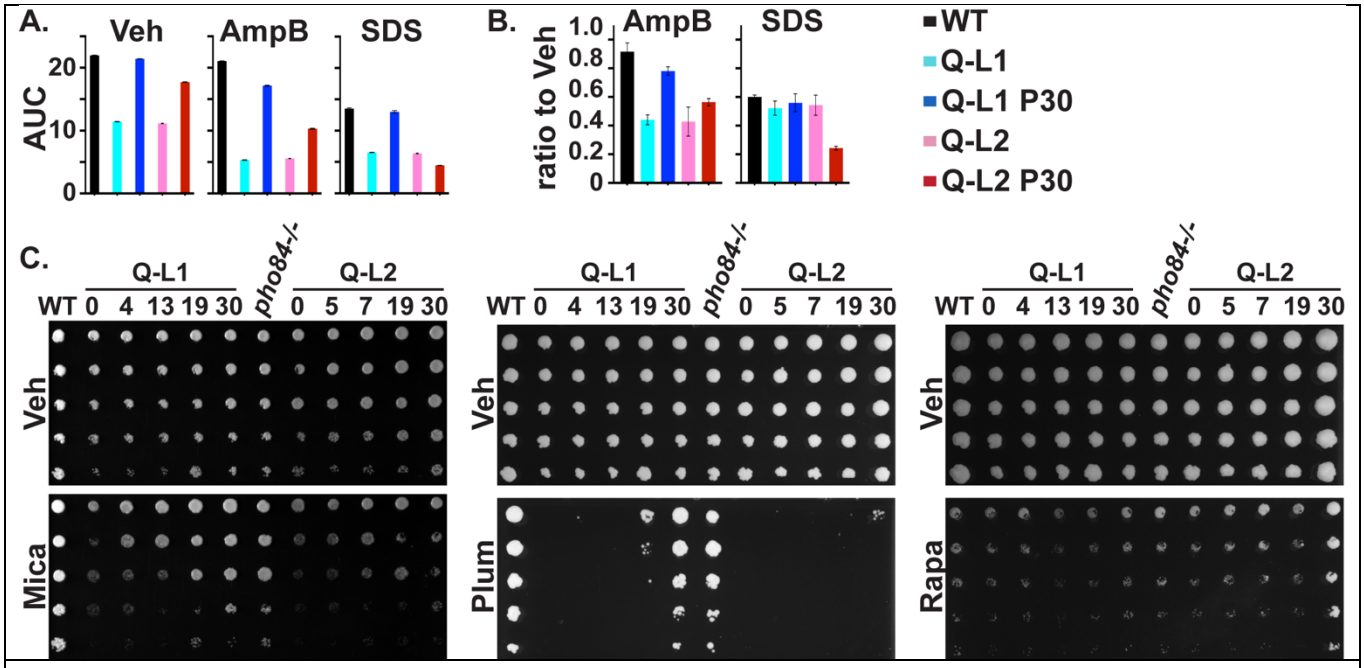

Fig. 9. Two evolving lineages of Q- cells showed distinct stressor endurance. A. Growth area under the curve (AUC) of cells grown in SC 1 mM Pi containing Vehicle (Veh, DMSO), 0.3 µg/ml Amphotericin B (AmpB) or 0.005% SDS. AmpB representative of 2 and SDS of 3 biological replicates; error bar SD of 3 technical replicates. **B**. Amphotericin B (AmpB) and SDS growth area under the curve (AUC) from panel A normalized to each strain's vehicle (Veh) control. WT (JKC915); Q-L1 (JKC2830); Q-L1 P30 (JKC2830 passage 30); Q-L2 (JKC2860); Q-L2 P30 (JKC2860 passage 30). AmpB average of 2 and SDS of 3 biological replicates; error bar SD of biological replicates. **C**. Threefold dilutions of cells of indicated genotypes, starting at OD_{600} 0.5, were spotted (top to bottom) onto SC medium containing Vehicle (Veh, H_2O) or 10 ng/ml micafungin (Mica), 15 µM plumbagin (Plum), 50 ng/ml rapamycin (Rapa), and grown at 30°C for 1 d (Mica), 2 d (Plum), 4 d (Rapa), respectively. Strains are WT (JKC915); Q-L1 (JKC2830) passage 0, 4, 13, 19, 30 and Q-L2 (JKC2860) passages 0, 5, 7, 19, 30; *pho84-/-* (JKC1450). JKC2830 and JKC2860 genotypes are *pho84-/- pho87-/- pho89-/- fgr2-/-*.

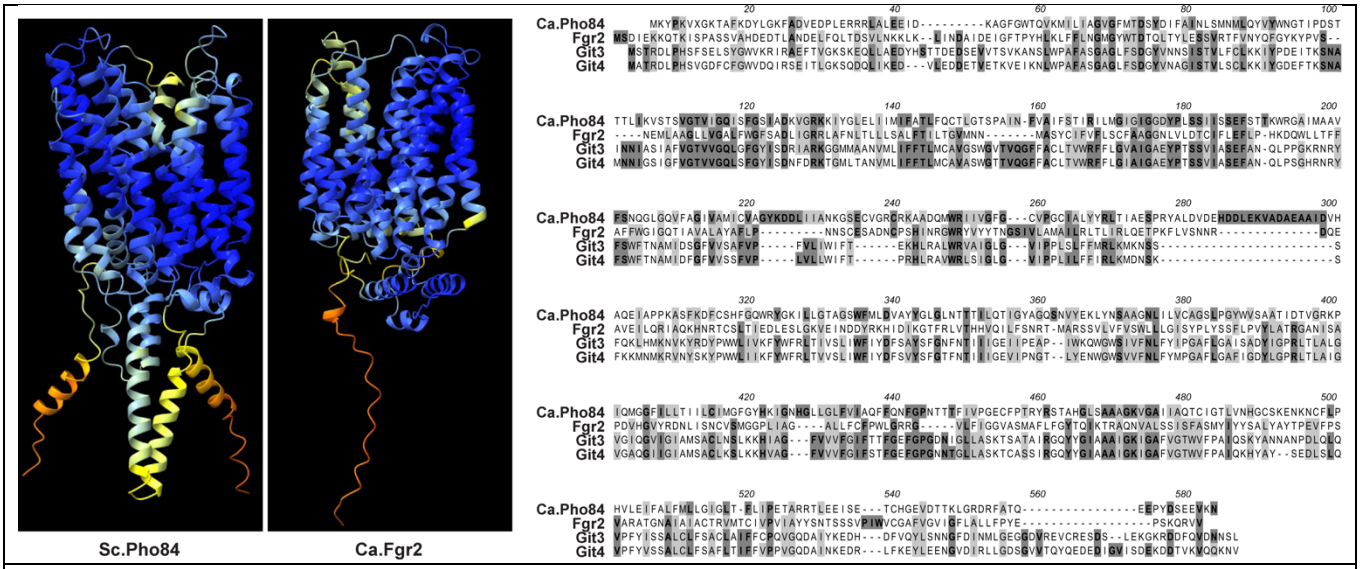

S1 Fig. Structural comparisons of Pho84 and its homologs. AlphaFold structure prediction of *S. cerevisiae* Pho84 and *C. albicans* Fgr2 was obtained from the AlphaFold Protein Structure Database (https://alphafold.ebi.ac.uk/) and visualized in ChimeraX-1.4. The coloring of each model is based on a per-residue confidence score (pLDDT): dark blue – very high (pLDDT > 90), light blue – confident (90 > pLDDT > 70), yellow – low (70 > pLDDT > 50), orange – very low (pLDDT < 50). Inorganic phosphate transporters were aligned in MacVector; identical amino acid residues tinted with dark gray and chemically similar ones in light gray.

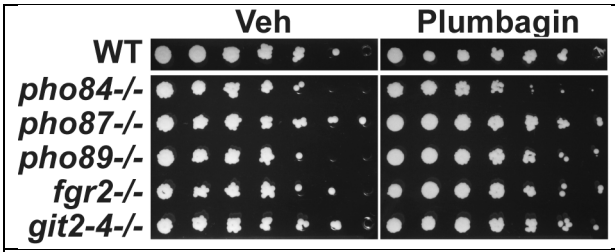

S2 Fig. Among Pi transporters, only Pho84 was required for oxidative stress endurance. Cell suspensions of the indicated genotypes WT JKC915; *pho84-/-* (JKC1450); *pho87-/-* (JKC2581); *pho89-/-* (JKC2585); *fgr2-/-* (JKC2667) and *git2-4-/-* (JKC2963) were spotted in 3-fold dilution steps onto SC medium with DMSO (Veh) or plumbagin 15 µM. Plates were incubated for 2 days at 30° C. Representative of 3 biological replicates. All spots were on the same plate.

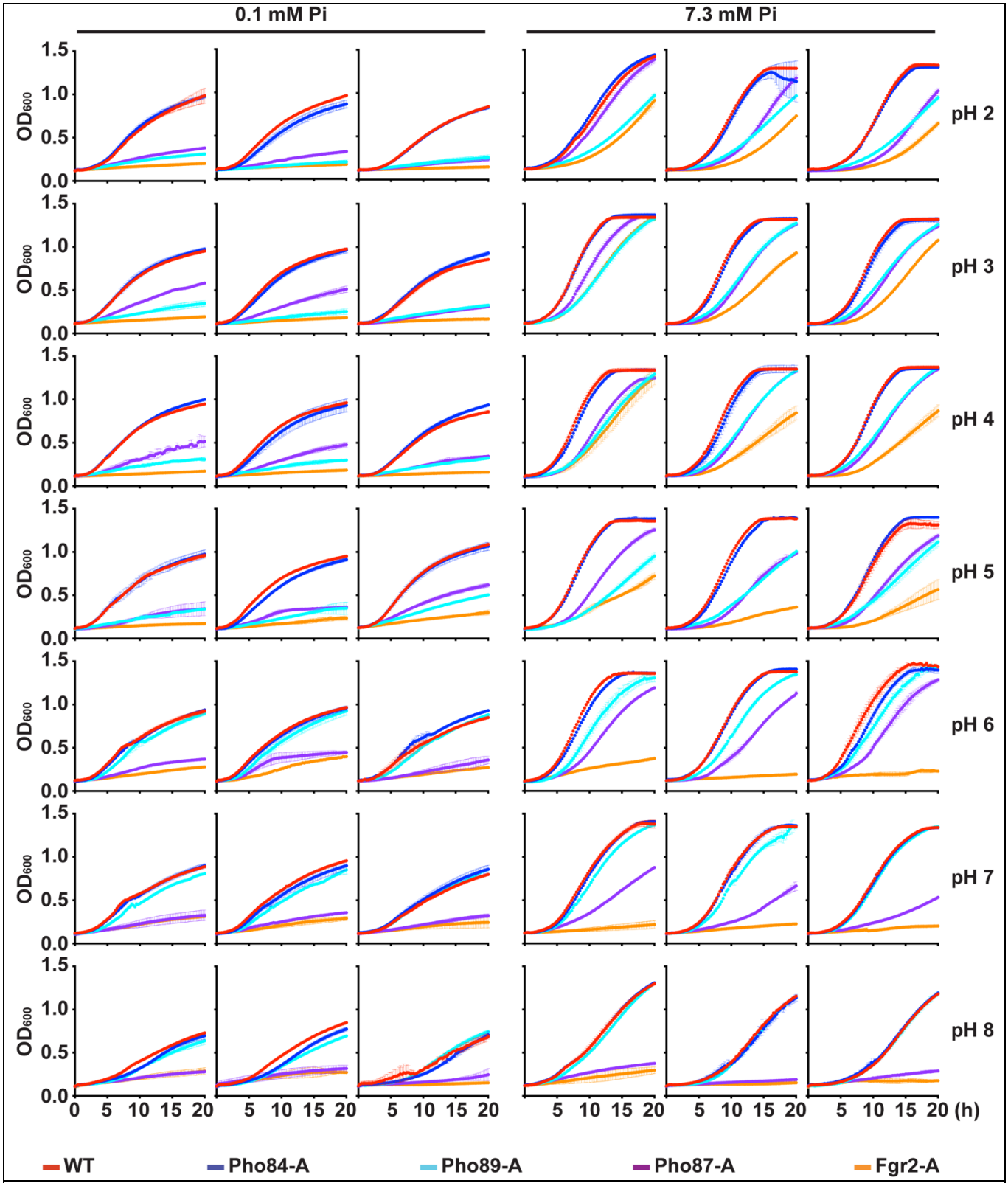

S3 Fig. Individual growth curves summarized in Figure 4. Strains were grown as described in Fig. 4. Shown are 3 biological replicates performed on different days. Error bars SD of 2 or 3 technical replicates. Strains are WT (JKC915); Pho84-A: *pho87-/- pho89-/- fgr2-/- PHO84+/+* (JKC2788); Pho87-A: *pho84-/- pho89-/- fgr2-/- PHO87+/+* (JKC2777); Pho89-A: *pho84-/- pho87-/- fgr2-/- PHO89+/+* (JKC2783); Fgr2-A: *pho84-/- pho87-/- pho89-/- FGR2+/+* (JKC2758).

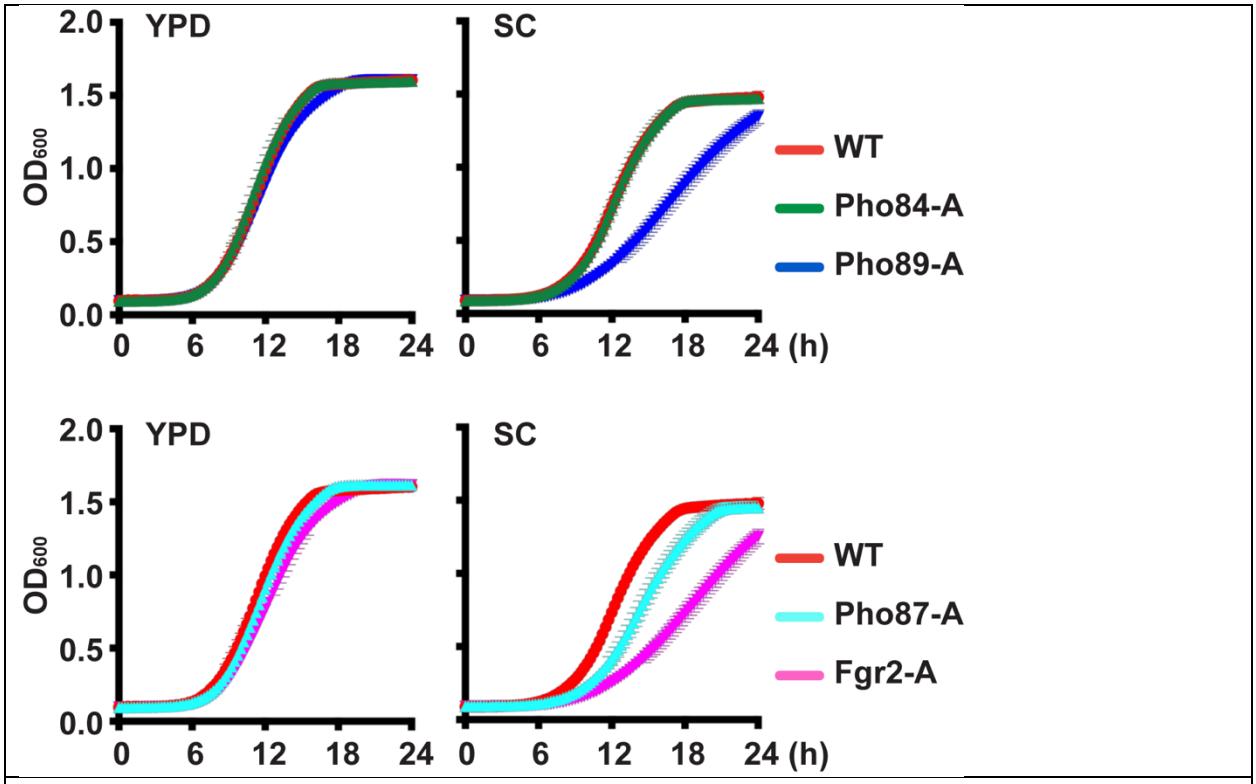

S4 Fig. Pi transporter triple mutants had no growth defects in rich complex medium. Cells of indicated triple mutant genotypes were grown in YPD (left) and SC (right) and OD_{600} was monitored. Upper panels: strains expressing only one of 2 high-affinity transporters. Lower panels: Strains expressing only one of 2 low-affinity transporters. Pho84-A: *pho87-/- pho89-/- fgr2-/- PHO84+/+* (JKC2788); Pho89-A: *pho84-/- pho87-/- fgr2-/- PHO89+/+* (JKC2783); Pho87-A: *pho84-/- pho89-/- fgr2-/- PHO87+/+* (JKC2777); Fgr2-A: *pho84-/- pho87-/- pho89-/- FGR2+/+* (JKC2758). Representative of 3 biological replicates; error bars SD of 3 technical replicates.

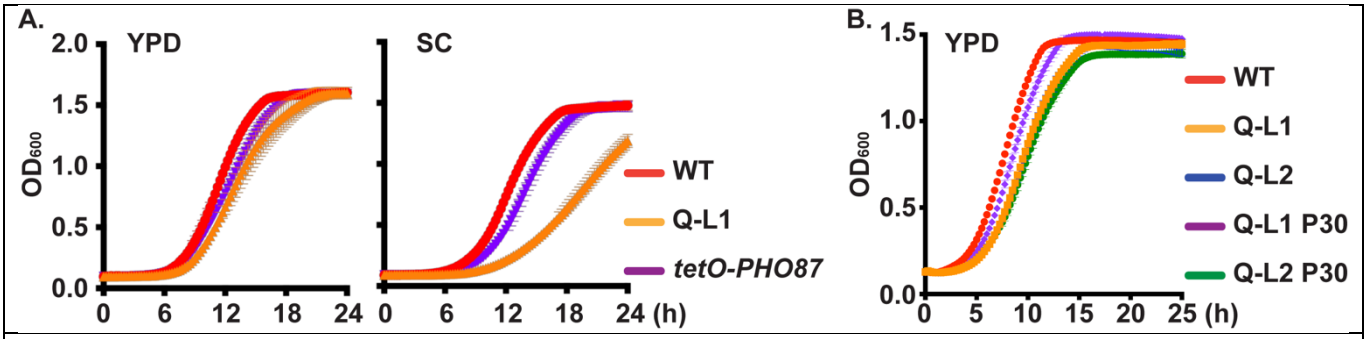

S5 Fig. Cells whose single Pi transporter was expressed from *tetO*, as well as Q- cells and their Pi scarcity-evolved descendant populations had no substantial growth defects in rich complex medium. Strains were grown as in S4 Fig. **A.** Cells in which a single allele of one Pi transporter, *PHO87*, is expressed from repressible *tetO*, were grown in YPD and SC without doxycycline and compared with WT and Q- cells. WT (JKC915), Q-L1 (*pho84-/- pho89-/- pho87-/- fgr2-/-*, JKC2830), *tetO-PHO87* (*tetO-PHO87/pho87 pho84-/- pho89-/- fgr2-/- git2-4-/-*, JKC2969). **B.** Growth in YPD of WT (JKC915); Q-L1 (JKC2830) and Q-L2 (*pho84-/- pho89-/- pho87-/- fgr2-/-*, JKC2860). P30: population from the 30th Pi scarcity passage.